International Journal of Greenhouse Gas Control 64 (2017) 284–299

Contents lists available at ScienceDirect

International Journal of Greenhouse Gas Control

journal homepage: www.elsevier.com/locate/ijggc

Evaluating model complexity in simulating supercritical CO_2 dissolution, leakage, footprint, and reservoir pressure for three-dimensional hierarchical aquifer

Mingkan Zhang[a], Ye Zhang[a,*], Peter Lichtner[b]

[a] Dept. of Geology and Geophysics, University of Wyoming, Laramie, WY 82070, United States
[b] OFM Research, Inc., Redmond, WA 98053, United States

ARTICLE INFO

Keywords:
Dissolution
Fingering
Parallel computing
Design of experiment
Heterogeneity
Facies model
Complexity

ABSTRACT

A hierarchical fully heterogeneous aquifer model (FHM) provides a reference for developing and testing 3 facies-based hydrostratigraphic models (HSMs) each representing a CO_2 storage aquifer with reduced permeability (k) heterogeneity resolution: 8-unit, 3-unit, and 1-unit homogeneous models. Under increasing aquifer lnk variances (0.1, 1.0, 4.5), flow upscaling was conducted to calculate equivalent permeabilities for the HSMs. Within a Design of Experiment uncertainty analysis framework varying geothermal gradient, salinity of formation water, caprock permeability, and injection rate, CO_2 injection coupled to convective mixing was simulated by all models. In addition to the injection phase, all simulations were carried out for 2000 years using PFLOTRAN, a massively parallel, multiphase, multicomponent numerical simulator that ran on the NCAR-Wyoming Supercomputing Center's Yellowstone supercomputer. Simulation outcomes of the HSMs were compared to those of the FHM within their full parameter space, and four performance metrics were evaluated: dissolved CO_2, CO_2 leakage, plume footprint, and pore pressure evolution in response to injection and migration. Results suggest that aquifer variance, heterogeneity resolution, and salinity can all affect the development of fingering and convective mixing, and therefore the amount of dissolution storage. For the modeling choices and assumptions made in this study, the 3-unit HSM was found to be an all-around optimal model by capturing both the sensitivity of the FHM and the performance metrics under different reservoir storage or operational conditions. Implications for modeling long-term CO_2 storage in data-poor systems are discussed and future research indicated.

1. Introduction

Concerns over global climate change due to the greenhouse effect have stimulated interest in developing various technologies to reduce the concentration of greenhouse gases in the atmosphere, in particular, carbon dioxide (CO_2). Geological Carbon Sequestration (GCS) is one of the options proposed to reduce CO_2 emissions, whereby supercritical-phase CO_2 ($scCO_2$) is injected into subsurface geologic formations such as deep saline aquifers, depleted oil and gas reservoirs, and unminable coal seams. Among these options, deep saline aquifers are considered excellent storage targets due to their large pore volumes, wide geographical distribution (easy accessibility to CO_2 point sources), and burial depths (isolation from underground sources of drinking water). After $scCO_2$ is injected into a deep saline aquifer, it exists as a buoyant fluid that can percolate upwards through fissures or permeable pathways in caprock, posing a leakage risk. For secure CO_2 storage in deep saline aquifers, several trapping mechanisms have been identified: (1) if low-permeability caprock exists above the aquifer, structural/stratigraphic trapping can keep the injected CO_2 localized (IPCC, 2005; Li et al., 2012; Li and Zhang, 2014); (2) as $scCO_2$ migrates and moves through aquifer pore space, residual trapping can take place where some $scCO_2$ is retained by capillary forces (IPCC, 2005; Li et al., 2016); (3) if the formation brine is unsaturated with CO_2, $scCO_2$ can dissolve into brine; and (4) if the aquifer matrix contains reactive minerals, they can react with dissolved CO_2 to form new minerals (Gaus, 2010; Jun et al., 2013). In general, these mechanisms operate over increasing time scales (from years to millennia) and represent increasing levels of storage security (IPCC, 2005).

Because CO_2 dissolution can reduce and (eventually) eliminate the buoyancy drive thus contributing to storage security, convective mixing, also referred to as Rayleigh-Taylor-type instability, is of particular interest. During convective mixing, brine in contact with CO_2

* Corresponding author.
E-mail address: yzhang9@uwyo.edu (Y. Zhang).

http://dx.doi.org/10.1016/j.ijggc.2017.07.022
Received 13 January 2017; Received in revised form 5 June 2017; Accepted 30 July 2017

becomes denser than brine not in contact with CO_2, creating hydrodynamic instability, i.e., brine saturated with CO_2 becomes "negatively buoyant" and sinks to formation bottom (Ennis-King and Paterson, 2005; Pau et al., 2010; Riaz et al., 2005). The sinking plume may create convective cells whereby unsaturated brine is continuously brought up to the two-phase region to dissolve more CO_2 (Hassanzadeh et al., 2007). Though both diffusive and advective transport of dissolved CO_2 can occur in the reservoir, convective mixing is dominated by advective transport which can be orders of magnitude more efficient than diffusive transport. Theoretical, laboratory, and numerical simulation studies are aimed to characterize and quantify such a process over a range of spatial and temporal scales. While laboratory experiment can provide physical insights into mixing and can be used to verify theory and simulations (Agartan and Trevisan, 2015; Chevalier et al., 2015), they are limited by the scale of the experiment. Theoretical analysis has yielded analytical scaling relations and parameters to quantify such mixing, e.g., characteristics such as onset time, rate of plume growth, and the evolution of dissolved CO_2 flux have been investigated using linear stability analysis (Tilton et al., 2013; Tilton and Riaz, 2014). However, aquifer media were assumed homogeneous and mixing after the onset of convection was not easily elucidated by the scaling relations. Most studies also focused on the single-phase (brine) region whereby dissolved CO_2 mass flux is supplied by a diffusive boundary that lies beneath a static/hypothetical $scCO_2$ plume. However, rather than assuming a static interface, Chevalier et al. (2015) suggested that multiphase mass transfer needs to be explicitly incorporated to accurately model convective mixing. Martinez and Hesse (2016) further suggested that the two-phase region (i.e., the transition zone between $scCO_2$ and resident brine) can enhance dissolution by eliminating the mass transfer constraint of the diffusive boundary. Clearly, by influencing two-phase flow during and after CO_2 injection, multiphase parameters and processes can also play a role, e.g., multiphase flow functions, hysteresis, gravity segregation, and injection strategy (Nield et al., 2010).

Because numerical simulation provides the greatest flexibility in evaluating complex and coupled processes that determine dissolution, an overview of simulation studies quantifying long-term (hundreds to thousands of years) CO_2 dissolution in saline aquifers is presented. When modeling CO_2 dissolution in a homogeneous aquifer, Farajzadeh et al. (2007) and Islam et al. (2013) suggested that both the mass transfer rate and the propagation speed of the CO_2 concentration front increase with the Rayleigh number. Lu et al. (2009) compared several equations-of-state and solubility models in predicting the redistribution and migration of supercrtical and dissolved CO_2. These authors found that accurate modeling of CO_2 flow and dissolution requires accurate equation-of-state for mixture properties. Homogeneous models were also used to test the sharp-interface assumption (Court et al., 2012), examine the sensitivity of heat and mass transfer rates to reservoir geometry and operating conditions (Bouzgarrou et al., 2013), and assess the importance of coupled dissolution-diffusion-convection processes (Zhang, 2013). Dissolution storage has also been evaluated for aquifers with heterogeneous intrinsic permeability (k). Comparing numerical simulations to laboratory experiments, Chevalier et al. (2015) suggested that detailed k heterogeneity can significantly impact convective mixing, i.e., pattern, onset time, and CO_2 mass flux. Interestingly, while some studies suggest that heterogeneity can enhance dissolution (Farajzadeh et al., 2007; Ranganathan et al., 2012), others found that heterogeneity exerts the opposite effect (Chen et al., 2013; Flett et al., 2007). Moreover, sedimentary aquifers often exhibit complex, nested facies structures creating hierarchical heterogeneity (Barrash and Clemo, 2002; Soltanian and Ritzi, 2014; Zhang et al., 2006). In such aquifers, convective mixing can be suppressed by low-k facies and enhanced in high-k facies, and the connectivity of high-k facies is found to dominate finger propagation and thus dissolution (Soltanian et al., 2016).

Realistic assessment of long term CO_2 dissolution requires the solution of miscible two phase flow with an accurate equation-of-state for the CO_2-brine mixture density, while medium/small scale heterogeneity must also be accounted for (Gershenzon et al., 2015a). However, modeling long-term storage in three-dimensions (3D) using high resolution grids incorporating detailed heterogeneity is challenging. Many efforts have been made on improving computational efficiency in multiphase simulations while addressing unresolved heterogeneity with various stochastic and upscaling techniques. One idea is to develop simplified multiphase, multicomponent simulators that are capable of giving reasonably accurate results. For example, streamline simulations aim to efficiently simulate flow and transport in large and complex models by decoupling the computation of flow and transport; however, such techniques often neglect molecular diffusion and transverse dispersion that couple neighboring streamlines (Datta-Gupta and King, 2007; Juanes and Lie, 2007, 2006; Lazaro Vallejo et al., 2011; Qi et al., 2009a,b). Vertically integrated models are another class of reduced physics models, reducing 3D problems to 2D. By combining finite volume approaches for solving vertically averaged flow equations and analytical solutions to account for small scale processes, computational efficiency can be improved (Gasda et al., 2011, 2009); however, at the expense of vertical detail. Multi-physics methods (Class et al., 2008; Fritz et al., 2012; Niessner and Helmig, 2009) have been employed to ignore certain phases and components in the reservoir in order to reduce computational time. Although computational efficiency can be improved while achieving comparable accuracy as simulations without simplifications, these methods can be highly conditional requiring that regions where certain physical processes occur can grow or shrink during simulation and/or regions of different processes can be adequately coupled (Geiger et al., 2012b). Similarly, stochastic and upscaling techniques are developed because it is practically impossible to simulate field scale processes with a grid that captures all small scale heterogeneities, which would lead to prohibitively large models and computing times. Some of the stochastic techniques incorporate ideas such as adding a stochastic forcing term to the flux equation (Geiger et al., 2012; Tartakovsky, 2010; Tartakovsky et al., 2008; Tyagi et al., 2008; Tyagi and Jenny, 2011), employing a stochastic partial differential equation (Neuweiler et al., 2011), using continuous time random walks (Rhodes et al., 2008), and utilizing pore-scale/continuum-scale hybrid methods (Battiato et al., 2011; Ryan and Tartakovsky, 2011). Upscaling techniques have also been developed in studying CO_2 dissolution. A flow-based upscaling method was used to capture the details generated by small-scale k heterogeneities in CO_2 dissolution simulations (Flett et al., 2007; Hidalgo et al., 2013; MacMinn et al., 2012). Alternatively, Elenius and Gasda (2013) and Gasda et al. (2013, 2012) developed an upscaling model based on the vertical equilibrium assumption to develop a vertically-integrated approach to study CO_2 migration and immobilization. Finally, to represent hierarchical aquifers, different k heterogeneity representations were compared in simulating the same CO_2 injection test and post-injection migration (Li et al., 2012). Results suggest that a higher heterogeneity resolution is required for predicting plume shape than for predicting reservoir pressure and brine leakage. However, the effect of heterogeneity resolution on dissolution was not examined.

This study evaluates the long-term interplay between heterogeneity resolution, two-phase flow, and convective mixing in predicting CO_2 performance metrics such as dissolution, leakage, footprint, and pore pressure. The study is based on a set of synthetic aquifer models including a high resolution *reference* fully heterogeneous model (FHM) whose permeability connectivity is captured at various scales to create 3 facies-based hydrostratigraphic models (HSMs). The HSMs capture heterogeneity at different "geologic resolutions", considered analogous to conceptual site models built with varying amount of characterization data (thus cost). Because natural aquifers often exhibit weak to strong variability, the FHM was populated with ln$k$ at increasing variances. At a given ln$k$ variance, a global upscaling technique was employed to compute equivalent permeabilities for the HSMs. CO_2 injection was

then simulated with all models and the predicted performance metrics compared. By incorporating miscibility in modeling two-phase flow, we aim to understand if the lower resolution HSMs can provide reasonable estimates of *the full suite* of the performance metrics. Model comparisons were carried out within a designed parameter space using an efficient sensitivity analysis technique (Li and Zhang, 2014), thus we also aim to evaluate if the HSMs can capture the sensitivity of the FHM under reservoir and operational uncertainty. Finally, to improve computation efficiency, CO_2 storage was simulated using PFLOTRAN, a massively parallel, multiphase, multicomponent, non-isothermal subsurface fluid flow simulator (Lichtner et al., 2013). All simulations were run on the NCAR-Wyoming Supercomputing Center's Yellowstone supercomputer, a petaflop high-performance IBM iDataPlex cluster with 72,576 processor cores and 144.6 TB of memory (CISL, 2013). In PFLOTRAN, miscible two-phase flow is simulated with instantaneous imposition of equilibrium between brine and $scCO_2$. The need for a diffusive CO_2 mass flux boundary, required for miscible single-phase simulation, is eliminated. All models were discretized with the same high resolution grid. Issues associated with grid coarsening are not addressed.

In the remainder of this article, model construction is described first, followed by brief presentations of the upscaling method, PFLOTRAN description, and the uncertainty analysis. Results comparing all models for calculating key CO_2 performance metrics are presented. For each model, important parameters that have a first order impact on storage and leakage are identified. For the given set of modeling choices and assumptions, an "optimal" heterogeneity resolution is identified which leads to model simplification. Implications for modeling long-term CO_2 storage in data-poor systems are discussed and future research indicated.

2. Methods

Injection of $scCO_2$ was simulated using synthetic models of a target storage aquifer, its caprock, and an overlying aquifer (Fig. 1a). The model dimensions are of field scales to accommodate the evolution of $scCO_2$ footprint simulated for 2000 years. Both caprock and overlying aquifer are assumed homogeneous while the target aquifer is populated with heterogeneous k at decreasing resolutions: (1) reference FHM (Fig. 1b); (2) an 8-unit HSM (Fig. 1c); (3) a 3-unit HSM (Fig. 1d); (4) a 1-unit HSM (see the layer-cake configuration of Fig. 1a). Compared to the FHM, the HSMs with reduced resolutions were constructed to represent models built using limited and/or low-resolution site data. The top boundary of all models is set at 2 km below land surface. For all models, CO_2 injection and post-injection monitoring were simulated under identical conditions. Within an efficient global uncertainty analysis framework, a set of input parameters were varied and those with a significant impact on dissolution and leakage were identified. Below, the methods used to create the models, the equations solved to simulate $scCO_2$ injection and storage, and the uncertainty analysis method are explained.

2.1. Creation of the synthetic models

This study uses stratigraphic data exhibiting hierarchical heterogeneity that reflects physical sedimentation processes in a laboratory flume (Sheets et al., 2002; Zhang et al., 2010). By scanning the deposit at high resolution and aligning the scanned images, a reference FHM was created. This model was scaled to field dimensions (Fig. 1a) to create a target aquifer with k variation that mirrors sedimentation (each local k was assumed isotropic). Because highly resolved discretization is needed to minimize numerical dispersion that can obscure or interfere with the simulation of fingering, each image pixel (i.e., at mm scale in the laboratory) is scaled to a model grid block: $\Delta x = \Delta y = 20$ m and $\Delta z = 10$ m. The target aquifer is discretized as: 250 (in x) × 250 (in y) × 40 (in z), or 2.5 million block cells. The full model, including the caprock and overlying aquifer, has $L_x \times L_y \times L_z = 5000 \times 5000 \times 600$ m^3 and 250 (in x) × 250 (in y) × 60 (in z) or 3.75×10^6 block cells.

To represent storage aquifers with increasing variability, ln$k$ variance (σ^2) of the FHM was scaled from 0.1, to 1.0, to 4.5 (when $\sigma^2 = 4.5$, k varies over 10^6). During this scaling, mean ln$k$ of the distribution was fixed corresponding to average sandstone permeability (this value is also assigned to the homogeneous aquifer overlying the caprock). A heterogeneous porosity field was then computed using a representative log$k$-porosity transform for sandstones (Ertekin et al., 2001). To create the HSMs, an image processing algorithm (Parker, 2010) was used to map the k connectivity of the FHM to capture distinct facies (8-unit model), before facies of similar k values were grouped into depositional environments (3-unit model). The 1-unit model then grouped all depositional environments into a homogeneous target aquifer. The algorithm, by adopting cutoffs from the k distribution of the FHM, can create an arbitrary number of facies. The 8-unit model is considered a reasonable representation of facies grouping without distinguishing extremely disconnected heterogeneity. All models employ the same high resolution grid, thus they vary only in how k of the target aquifer is represented. Porosity of each unit of the HSMs was computed by volume averaging those of corresponding cells in the FHM. In summary, 3 HSMs were created for each FHM for a given *ln$k$* variance. For the 3 variances tested, 12 models were created.

Because the FHM exhibits long-range k correlation, a global upscaling technique capable of capturing facies connectivity was used to compute an equivalent permeability tensor ($\boldsymbol{k}^*$) for each HSM unit (Zhang et al., 2011). For the 1-unit model, a single aquifer-scale $\boldsymbol{k}^*$ was computed. The upscaling procedure is: (1) the FHM was simulated solving the steady-state single phase incompressible flow equation under different global boundary conditions (BC), (2) for each unit, mean flux and hydraulic gradient were computed for each BC; (3) by imposing Darcy's Law using the computed mean fluxes and gradients from all BC, $\boldsymbol{k}^*$ was computed with a least-squares method. Given the aquifer variances investigated ($\sigma^2 = 0.1, 1.0, 4.5$), 3 sets of upscaled $\boldsymbol{k}^*$ were obtained for each HSM using 3 global BC to drive flow (i.e., x flow, y flow, and z flow, which drives fluid flow towards the positive x, y, and z axis, respectively). Though more BC can be explored in computing $\boldsymbol{k}^*$, our experience suggests that for a heterogeneity pattern that is largely parallel or perpendicular to the coordinate axes (Fig. 1b), linear flows can yield reasonably accurate $\boldsymbol{k}^*$ estimates for different facies geometries (Li et al., 2012; Zhang et al., 2006). Indeed, most of the computed $\boldsymbol{k}^*$ are diagonally dominant anisotropic full tensors with larger equivalent horizontal permeabilities than equivalent vertical permeabilities. This suggests that the effect of lateral stratification on flow has been captured. Accuracy of the upscaled $\boldsymbol{k}^*$ was assessed by comparing the hydraulic head distributions of the HSMs against that of the FHM for the different BC and ln$k$ variances (Fig. 2). In general, upscaling error in computing hydraulic head is found to be less than 10% and often much smaller, even when variance is high. Though not shown, error in flow rate recovery by the HSMs is similar. The 1-unit model has significantly larger errors: errors in both head and flow rate calculations often more than double those of the 3-unit model.

2.2. PFLOTRAN: massively parallel, multiphase-multicomponent flow & transport model

The computer code PFLOTRAN solves a coupled system of mass and energy conservation equations for two-phase flow consisting of $scCO_2$ and H_2O. PFLOTRAN describes coupled thermal-hydrologic-chemical (THC) processes in variably saturated, nonisothermal, porous media up to three spatial dimensions. For pure CO_2, the Span-and-Wagner equation-of-state, which has been accepted by NIST and is currently thought to be the most accurate formulation, is used (Span and Wagner, 1996). A lookup table algorithm is used to obtain density, fugacity, and fugacity coefficient of pure CO_2. Mixture density for CO_2 dissolved in brine is based on the equation-of-state presented in Duan et al. (2008).

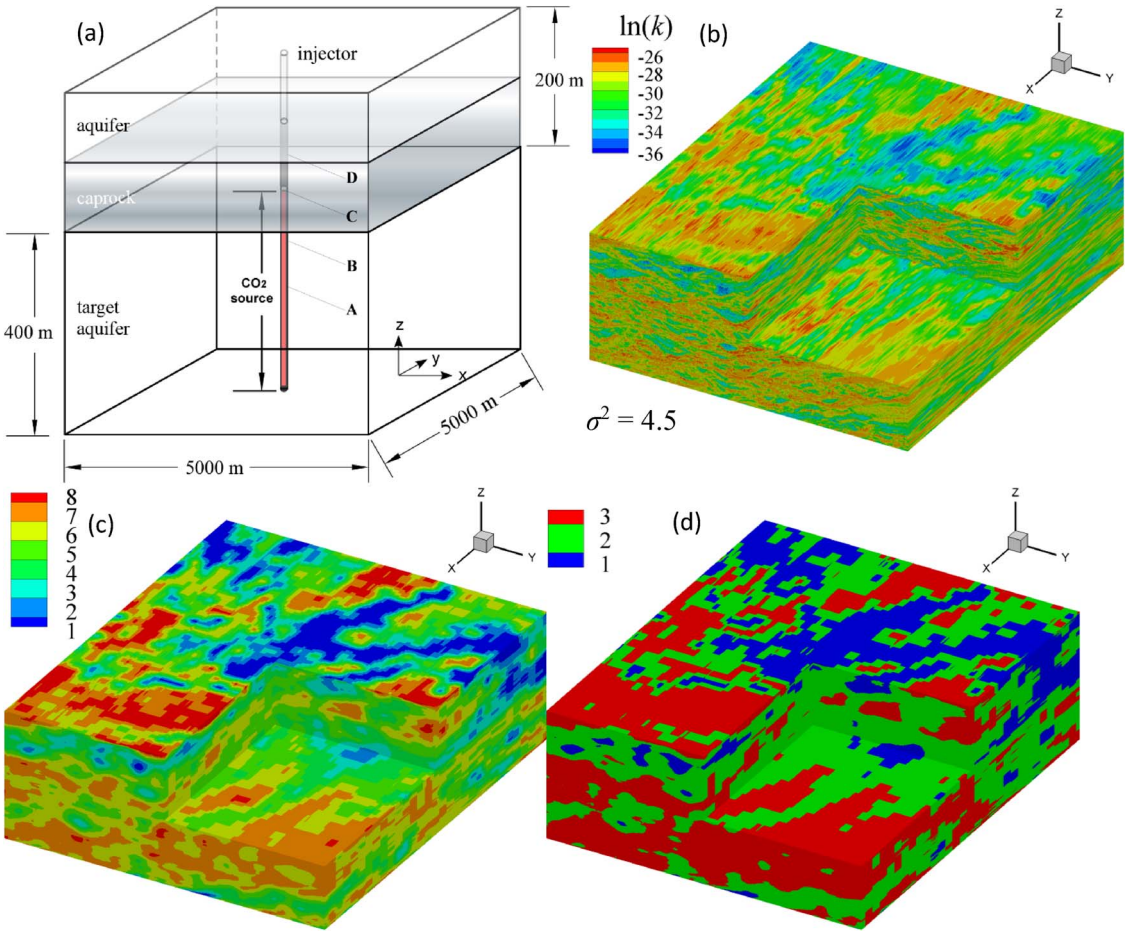

Fig. 1. (a) Schematic diagram of the model including a target aquifer, an overlying caprock, and a shallow aquifer. Locations of 4 observation points at the injection well are indicated: z = 205 (A), 305 (B), 395 (C) and 455 (D) m. (b) ln$k$ distribution of the FHM in the target aquifer at σ^2 = 4.5. Three cut planes reveal the complex internal heterogeneity created by fluvial-like depositional processes. (c) 8-unit hydrostratigraphic model with colors representing facies IDs. (d) 3-unit hydrostratigraphic model with colors representing facies IDs.

2.2.1. Mass and energy conservation equations

These conservation equations can be written as:

$$\frac{\partial}{\partial t}[\phi(s_l\eta_l X_i^l + s_g\eta_g X_i^g)] + \nabla\cdot[\boldsymbol{q}_l\eta_l X_i^l + \boldsymbol{q}_g\eta_g X_i^g - \phi(s_l D_l\eta_l\nabla X_i^l + s_g D_g\eta_g\nabla X_i^g)] = Q_i, \tag{1a}$$

$$\frac{\partial}{\partial t}[\phi(s_l\eta_l U_l + s_g\eta_g U_g) + (1-\phi)\rho_r c_r T] + \nabla\cdot[\boldsymbol{q}_l\eta_l H_l + \boldsymbol{q}_g\eta_g H_l - \kappa\nabla T] = Q_e. \tag{1b}$$

where l and g refer to liquid water (brine) and scCO$_2$ phases, respectively; species are designated by i = CO$_2$, H$_2$O; ϕ denotes an effective porosity; s_l and s_g refer to liquid and gas (scCO$_2$) saturation, respectively ($s_{l+}s_{g=1}$); $X_i^\alpha(\alpha = l, g)$ denotes the mole fraction of species i in fluid phase α ($X_{CO_2}^\alpha + X_{H_2O}^\alpha = 1$); D_l and D_g are dispersion coefficients in phase l and g, respectively, which are assumed species independent; T is temperature; η_α, H_α, U_α refer to the molar density, enthalpy, and internal energy of phase α, respectively; the source/sink terms describe mass (Q_i) and energy (Q_e) injection and extraction at wells; $\boldsymbol{q}_\alpha$ denotes the phase Darcy velocity defined by:

$$\boldsymbol{q}_\alpha = -\frac{\boldsymbol{k}k_\alpha}{\mu_\alpha}(\nabla p_\alpha + \rho_\alpha g\nabla z) \tag{2}$$

where p_a is phase pressure, $\boldsymbol{k}$ is intrinsic permeability tensor, k_α denotes phase relative permeability, μ_α is the phase viscosity, ρ_α is the phase density, and $\boldsymbol{g}$ denotes the gravitational constant.

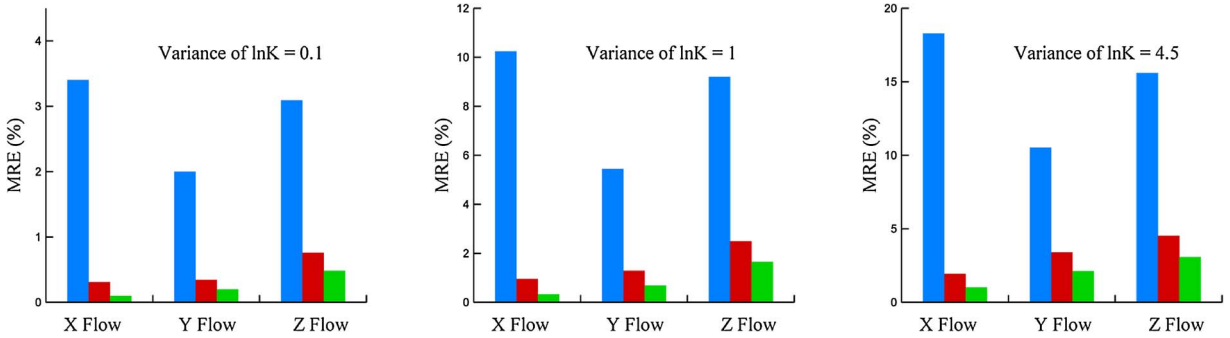

Fig. 2. Mean relative error (MRE) in the prediction of hydraulic head by the HSMs under different fluid flow boundary conditions. σ^2 = 0.1 (a), σ^2 = 1.0 (b), and σ^2 = 4.5 (c).

The liquid and gas pressures are related by the capillary pressure p_c

$$p_l = p_g - p_c, \tag{3}$$

where the capillary pressure is given in terms of an effective liquid saturation:

$$p_c = \frac{1}{\alpha}[(s_l^e)^{1/m} - 1]^{1-m}, \tag{4}$$

where the effective liquid saturation is defined as:

$$s_l^e = \frac{s_l - s_l^r}{1 - s_l^r}, \tag{5}$$

where s_l^r denotes the residual liquid saturation, and α and m are van Genuchten parameters. Relative permeabilities for liquid water H_2O and $scCO_2$ are based on the van Genuchten relations:

$$k_{H_2O}^r = \sqrt{s_l^e}\,[1 - (1 - (s_l^e)^{1/m})^m]^2, \tag{6a}$$

$$k_{CO_2}^r = \sqrt{1 - s_l^e}\,[1 - (1 - (s_l^e)^{1/m})^m]^2. \tag{6b}$$

Henry's law is used to calculate the dissolved CO_2 concentration in an NaCl brine based on the correlation presented in Duan and Sun (2003).

2.2.2. Initial and BC

Before CO_2 injection, the storage system was initially saturated with brine of a given salinity (see 2.3). The initial pressure and temperature distributions were set based on depth, hydrostatic pressure, and geothermal gradient (see 2.3). Boundary conditions of the simulation are set as: no-flow at the top and bottom boundaries; hydrostatic pressure profile at the sides, which allows the resident brine, and later CO_2, to flow out of the model. For the chosen BC and the relatively low injection rate (see 2.3), pressure buildup in all models during CO_2 injection was modest and reservoir geomechanical response was not considered. Thermal BC include fixed temperatures at the top and bottom boundaries, assigned based on depth and geothermal gradient. A fixed temperature profile was specified at the sides using the same geothermal gradient.

2.2.3. Solution method

According to the Gibbs phase rule, there are $N_C + 1$ ° of freedom in a multiphase, multicomponent system, where *Nc* is the number of independent primary variables. For the two-phase, two-component system modeled here, there are 2 + 1 = 3 ° of freedom. The choice of the independent primary variables depends on the phases present. To select the set of primary variables at each grid cell, a variable switching approach was used. For pure water, the primary variables consist of the set (p_l, T, $X_{CO_2}^l$). For pure gas, the primary variables consist of the set (p_g, T, $X_{CO_2}^g$). For the two-phase system H_2O-$scCO_2$, the primary variables consist of the set (p_g, T, s_g). Phase transitions may occur from pure liquid water and gas to two-phase, and vice versa (Table 1). Eqs. (1a) and (1b) were discretized using a finite volume approach; the resulting system of nonlinear algebraic equations was solved using a fully implicit Newton-Raphson method.

Table 1
Phase transition rules employed in PFLOTRAN.

Phase Transition	Condition	Variable Change
$l \rightarrow lg$	$\mu_{CO_2}^l \le \mu_{CO_2}^g$	$(p_l, T, X_{CO_2}^l) \rightarrow (p_g, T, s_g)$
$g \rightarrow lg$	$\mu_{CO_2}^l \ge \mu_{CO_2}^g$	$(p_g, T, X_{CO_2}^g) \rightarrow (p_g, T, s_g)$
$lg \rightarrow l$	$s_g \le 0$	$(p_g, T, s_g) \rightarrow (p_l, T, X_{CO_2}^l)$
$lg \rightarrow g$	$s_g \ge 1$	$(p_g, T, s_g) \rightarrow (p_g, T, X_{CO_2}^g)$

2.2.4. Parallel implementation

PFLOTRAN is developed from the ground up to run on architectures ranging from laptops to massively parallel supercomputers. Parallelization is implemented through the PETSc library (Balay et al., 1997). PETSc provides a user friendly set of parallel routines for solving systems of nonlinear equations using domain decomposition. These include parallel solvers and preconditioners, parallel construction of the Jacobian matrix and residual function, and seamless message passing, which together provide a high parallel efficiency. For a 3D test case simulating injection of $scCO_2$ into an arkosic sandstone, parallel speedup for PFLOTRAN running on the Yellowstone supercomputer at the National Center for Atmospheric Research's computing facility located at Cheyenne, WY, with up to 8192 processor cores, is shown in Fig. 3. In solving this problem, reactions from the dissolved CO_2 with a set of minerals were additionally simulated. Ten time steps for flow and transport were taken to create the speedup curve. A grid with dimensions of 500 × 500 × 100 with a 1-m grid spacing and with 3 and 10 equations per node for flow and transport, respectively, giving 75×10^6 (flow) and 325×10^6 (flow coupled to transport) total degrees of freedom, was used. The speedup curve suggests that good performance gain was achieved on Yellowstone for CO_2 modeling. All modeling of this study was carried out on Yellowstone.

2.3. Uncertainty analysis

Uncertainty analysis is based on the Design of Experiment (DoE) sensitivity analysis which can be used to efficiently explore parameter space (Montgomery, 2008; Yeten et al., 2005). This methodology has been utilized in the uncertainty analysis of oil reservoirs and CO_2 storage systems (Li and Zhang, 2014; Milliken et al., 2008; Zhang et al., 2014), where the input parameters to a simulator can remain fixed (those that typically vary little at a storage site) or variable (those that are typically uncertain or can assume a range of operating conditions/values). The latter group of parameters, often called design factors, are varied in the DoE analysis. As our earlier works (e.g., Li and Zhang, 2014) have provided more detailed discussion of this methodology, only a brief explanation is presented here.

In the DoE analysis, a subset of factors are varied simultaneously according to a design table. These factors can be continuous or categorical, the latter can be modeling choices. Though various designs are available (the same design can be used for analyzing multiple outcomes), a 3-level Box–Behnken design was used here. When the number of factors is limited (generally less than 10), this design can provide a sufficient level of resolution using limited simulations to identify a set of key factors that impact a particular outcome at a user-specified significance. Results of the simulations are then compiled and analyzed with multivariate analysis of variance (MANOVA), which ranks the factors in terms of their importance on influencing an outcome.

For the uncertainty analysis of this study, Table 2 lists the input factors and their ranges: (1) temperature gradient; (2) brine salinity, (3) caprock permeability, and (4) CO_2 injection rate. Each factor is given 3 levels, as required by the Box-Behnken design. The selection of the factors and their ranges reflects generic rather than site specific conditions. The factors were considered independent of aquifer heterogeneity, and were therefore varied *identically* for each model. Because the injection rate was variable, the injection duration was modified to ensure that the total injected CO_2 mass was the same for all simulations. For example, injection spans 40 years for a rate of 2 kg/s, 20 years for 4 kg/s, and 10 years for 8 kg/s. The total CO_2 injected is 2.523 Million tons. To achieve a higher rate in a target aquifer, particularly one with a wider (or lower) k ranges, multiple injectors are likely needed and pressure buildup can be controlled by brine production (Li et al., 2012). The complex scenarios involving multiple injectors and producers are not evaluated, though our study approach is easily extendable to such cases. Furthermore, because the total CO_2 injected is the same for all models (Table 2), this facilitates model comparison when pressure,

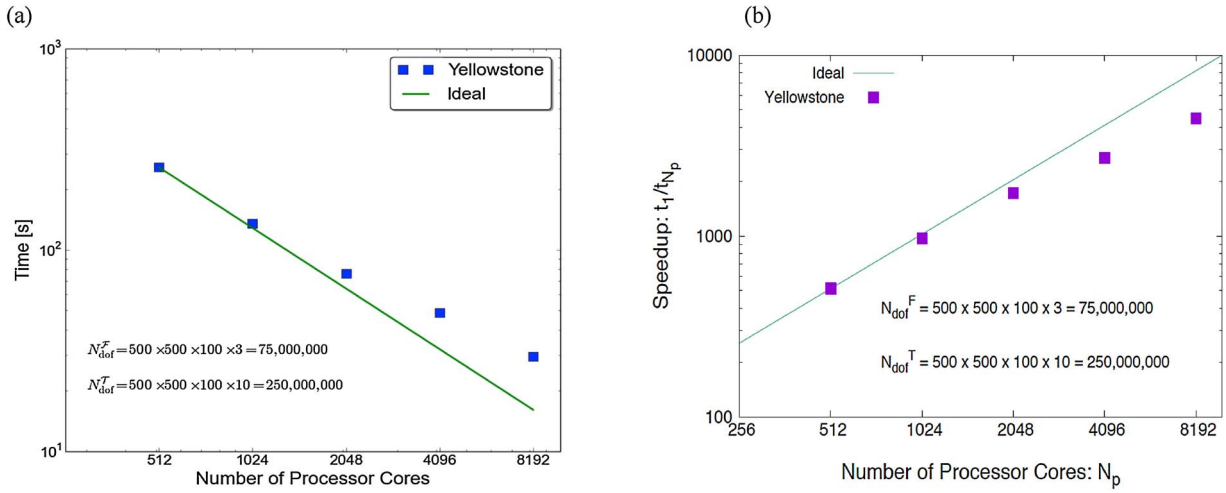

Fig. 3. Timing (a) and speedup (b) curves for PFLOW and PTRAN on the NWSC's Yellowstone supercomputer for a 3D grid 500 × 500 × 100 with 3 ° of freedom per node for two-phase flow simulation and 10 ° of freedom per node for reactive transport simulation. N_{dof} is the number of degrees of freedom. t_1 is the wall-o'clock-time for executing the parallel simulator on a single processor.

Table 2
Uncertain input parameters varied in the DoE analysis. The same set of simulations were conducted by each conceptual model.

Case	T Gradient (°C/m)	Brine Salinity (Molal)	k_{cap} (m^2)	Inject rate (kg/s)
1	−0.025	0	$10^{-17.5}$	4
2	−0.025	4	$10^{-17.5}$	4
3	−0.05	0	$10^{-17.5}$	4
4	−0.05	4	$10^{-17.5}$	4
5	−0.0375	2	10^{-16}	2
6	−0.0375	2	10^{-16}	8
7	−0.0375	2	10^{-19}	2
8	−0.0375	2	10^{-19}	8
9	−0.025	2	$10^{-17.5}$	2
10	−0.025	2	$10^{-17.5}$	8
11	−0.05	2	$10^{-17.5}$	2
12	−0.05	2	$10^{-17.5}$	8
13	−0.0375	0	10^{-16}	4
14	−0.0375	0	10^{-19}	4
15	−0.0375	4	10^{-16}	4
16	−0.0375	4	10^{-19}	4
17	−0.025	2	10^{-16}	4
18	−0.025	2	10^{-19}	4
19	−0.05	2	10^{-16}	4
20	−0.05	2	10^{-19}	4
21	−0.0375	0	$10^{-17.5}$	2
22	−0.0375	0	$10^{-17.5}$	8
23	−0.0375	4	$10^{-17.5}$	2
24	−0.0375	4	$10^{-17.5}$	8
25	−0.0375	2	$10^{-17.5}$	4

storage, leakage, and footprint are compared (at a given variance level). Finally, two long-term performance metrics – CO_2 dissolution and leakage at the end of simulation – were evaluated with MANOVA using JMP11.0 to rank the statistically significant factors that influence each metric at 95% confidence.

3. Results

For increasing variability (σ^2 = 0.1, 1.0 and 4.5), long term CO_2 storage and leakage were simulated by all models. At a given variance, 25 long-term simulations were carried out by each model (Table 2). For the 3 variances, 300 simulations were conducted. The total CPU time running the simulations on the NCAR-Wyoming Supercomputing Center's Yellowstone supercomputer is estimated at ~0.6 million core hours. Under factor combinations that together explore the parameter space, the HSMs were evaluated in their ability to capture key performance metrics of the FHM, e.g., CO_2 dissolution and leakage, footprint, and pore pressure response. For each model, results of the DoE analysis were also used to identify important factors that have statistically significant impact on each metric. The HSMs were evaluated in their ability to capture the ranking of the factors for the FHM.

3.1. Dissolution and leakage

CO_2 dissolution and leakage provide quantitative indicators of the benefit and risk of GCS. Fig. 4 presents dissolved CO_2 profiles computed by all models for cases 1 and 2 under increasing aquifer variances. The only difference between the two cases is the salinity of the formation water (0 and 4 Molal for case 1 and 2, respectively). Several

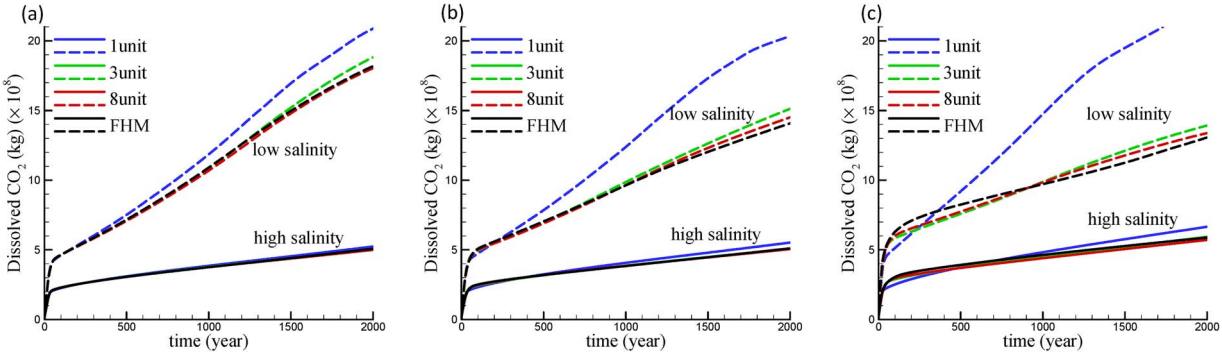

Fig. 4. Dissolved CO_2 for case 2 (solid lines; high salinity) and case 1 (dashed lines; low salinity) with σ^2 = 0.1 (a), σ^2 = 1.0 (b), and σ^2 = 4.5 (c).

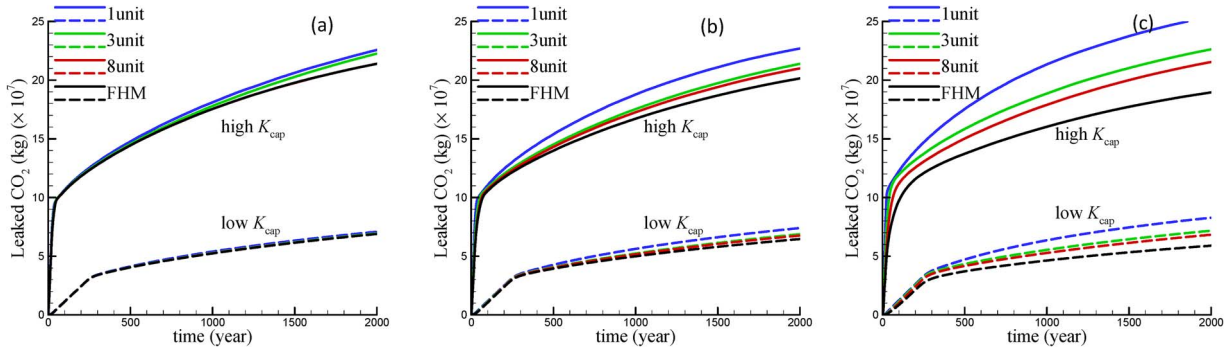

Fig. 5. Simulated CO_2 leakage into the caprock for case 18 (solid lines; high caprock permeability) and case 17 (dashed lines; low caprock permeability) with $\sigma^2 = 0.1$ (a), $\sigma^2 = 1.0$ (b), and $\sigma^2 = 4.5$ (c).

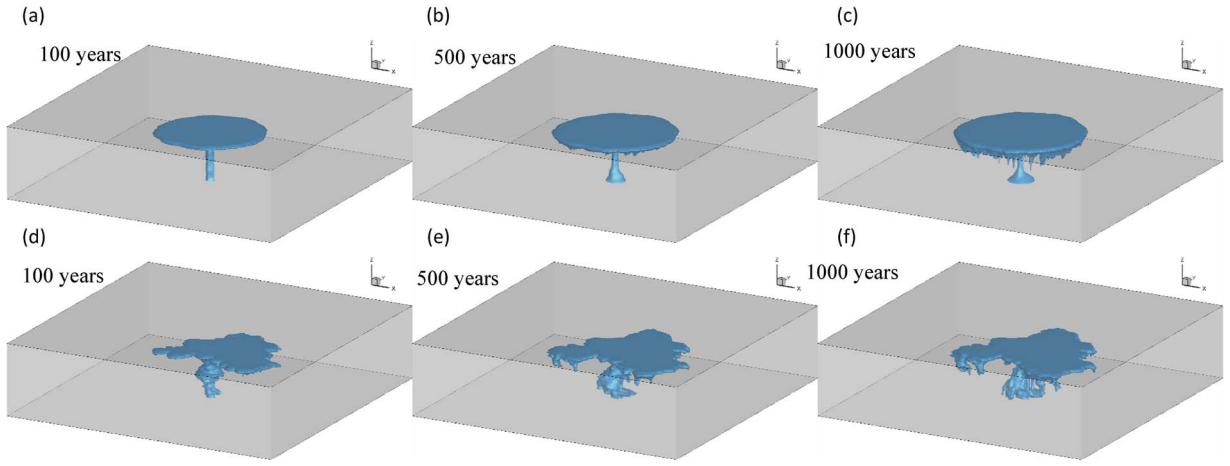

Fig. 6. Case 25: isosurface of dissolved CO_2 at 0.004 liquid mole fraction simulated by the FHM at 100 years, 500 years, and 1000 years with $\sigma^2 = 0.1$ (a–c) and $\sigma^2 = 4.5$ (d–f).

observations have been made: (1) for the parameter space explored, salinity has a first order impact on CO_2 dissolution: the amount of dissolved CO_2 in case 1 predicted by all models (dashed lines) is about 2–3 times that of case 2 (solid lines). (2) for all σ^2 and for all models, CO_2 dissolution increases with time, although the rate of dissolution changes. During injection, the rate is higher as formation water is undersaturated with $scCO_2$; after injection, CO_2 gradually dissolves into formation water when the leading edge of the plume slowly comes into contact with water under-saturated with CO_2. (3) For all variances, the 1-unit model predicts significantly more dissolution than all other models *when brine salinity is low*. Inspection of the dissolved CO_2 plume reveals that significant convective mixing has developed in this model, while convection is subdued in the other models due to the explicit representation of heterogeneity. When brine salinity is high, however, all HSMs including the 1-unit model predict similar total dissolved CO_2 as the FHM. This is because less CO_2 dissolution occurs and there is less density contrast between brine saturated with CO_2 and fresh (undersaturated) brine. Thus, high salinity suppresses convective mixing, and as a result, all models predict similar dissolution regardless of heterogeneity resolution. (4) At any variance, and for both low and high salinities, the 3-unit and 8-unit models calculated nearly identical amount of dissolution with mass errors (compared to the FHM) generally less than 5%. As expected, the higher the resolution in capturing aquifer heterogeneity, the better predictor a HSM is. This is true for calculating the other metrics as well, as discussed next.

Fig. 5 presents the amount of supercritical and dissolved CO_2 that has leaked into caprock and overlying aquifer as computed by all models, and, for all variances. This calculation is based on the fluxes of $scCO_2$ and dissolved CO_2 that have entered the caprock unit. Cases 17 and 18 are chosen to demonstrate leakage as they differ only in caprock permeability ($10^{-16}\,m^2$ for case 17 and $10^{-19}\,m^2$ for case 18). As expected, caprock permeability (k_{cap}) exerts a strong control on leakage: when k_{cap} is low, the amount of leakage is about 1/3 of the leakage from the high permeability case. For the given model geometry and the injection rates tested, a k_{cap} of $10^{-16}\,m^2$ leads to moderate leakage. For example, the FHM predicted that approximately 0.22Mt of CO_2 leaked into the caprock and overlying aquifer by the end of 2000 years. This is about 8.7% of the total CO_2 injected compared to only 2% of the total CO_2 injected when k_{cap} is $10^{-19}\,m^2$. Moreover, CO_2 was injected for 20 years for both cases 17 and 18. When k_{cap} is $10^{-16}\,m^2$, leaked CO_2 initially increases rapidly for about 20 years driven by pressure buildup, before the leakage rate declines and stabilizes. When k_{cap} is $10^{-19}\,m^2$, leakage rate is smaller and the onset of this transition time is longer (~300 years), reflecting a slower, diffusion-like process of mass transport into caprock. Finally, for both k_{cap} values, when heterogeneity is incorporated in the target aquifer, the predicted leakage becomes slightly reduced with increasing σ^2. When variance is higher (i.e., the low-k grid cells were assigned lower k values), low-k facies in the aquifer act to more strongly retard upward CO_2 migration. A smaller $scCO_2$ plume rises to the caprock, which leads to less leakage. When variance is lower, the aquifer is nearly homogeneous. During its upward migration, $scCO_2$ plume encounters less resistance, forming a larger footprint. However, when heterogeneity is ignored entirely (i.e., the 1-unit model), an opposite effect is observed which is attributed to this model's larger errors in capturing mean flow of the FHM.

3.2. Dissolved CO_2 plume

Dissolved CO_2 plumes simulated for case 25, where all 4 factors assume their median values (Table 2), are examined. Isosurfaces of dissolved CO_2 simulated by the FHM exhibit significant differences between those of the lowest (Fig. 6a–c) and highest (Fig. 6d–f)

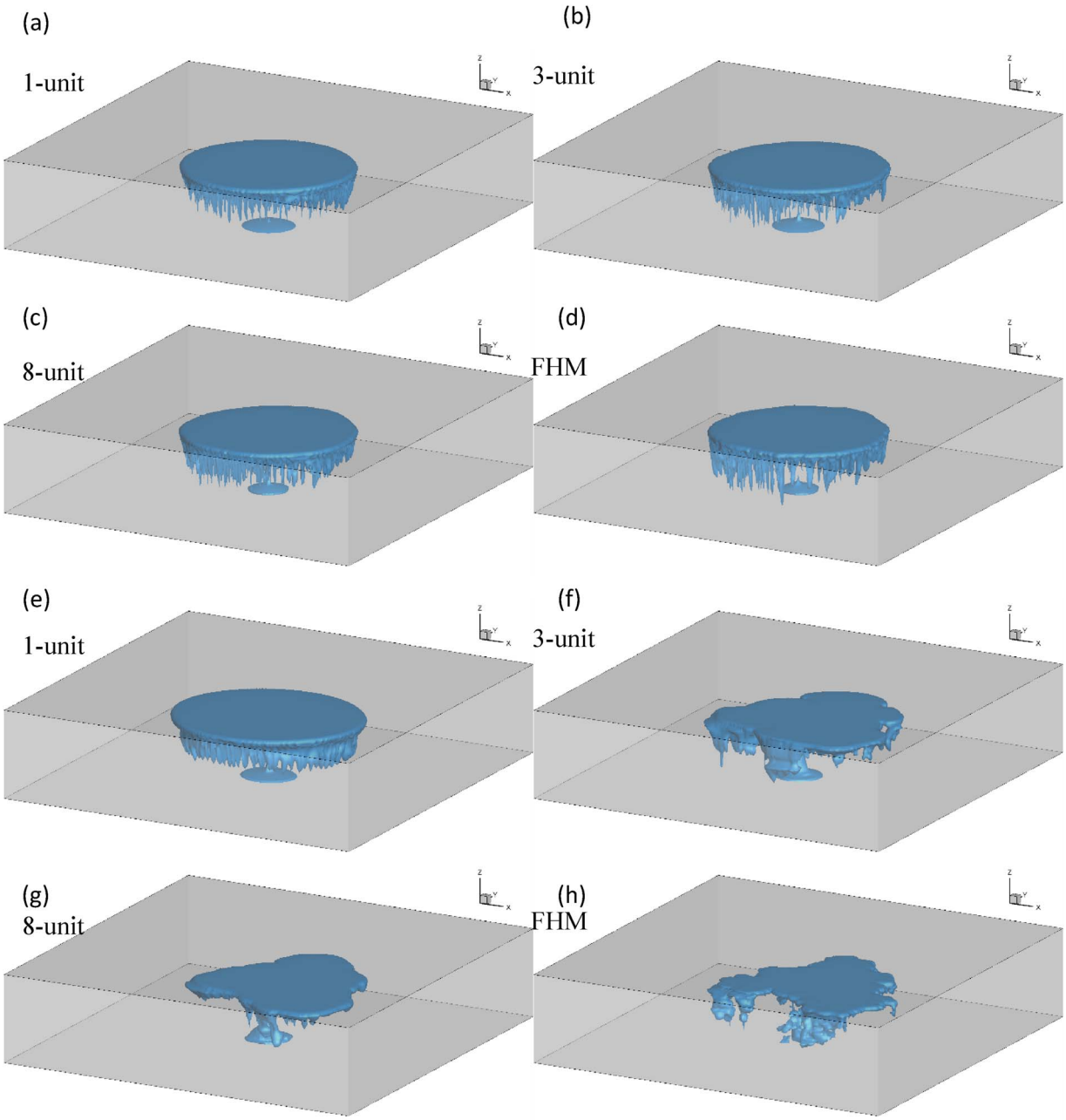

Fig. 7. Case 25: isosurface of dissolved CO_2 at 0.004 liquid mole fraction simulated by all models at 2000 years with $\sigma^2 = 0.1$ (a–d) and $\sigma^2 = 4.5$ (e and h).

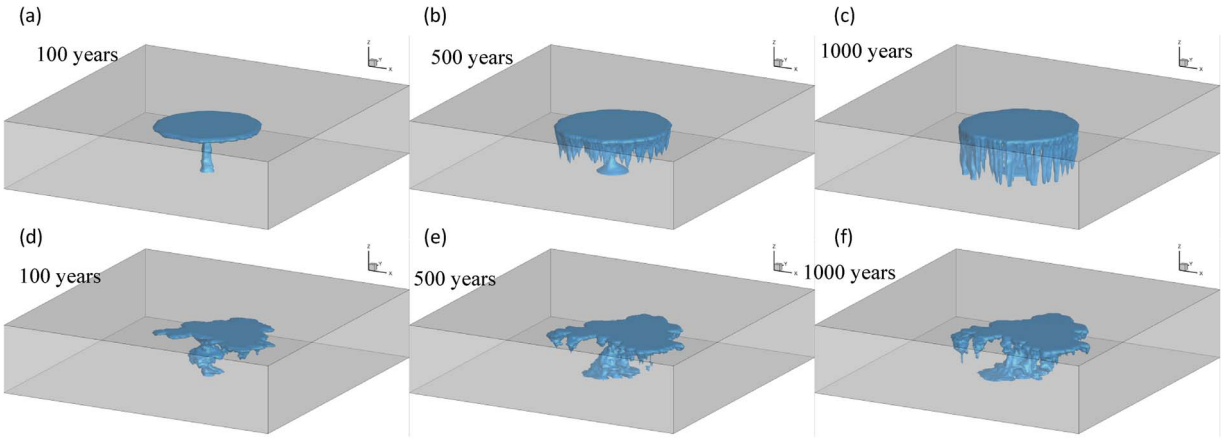

Fig. 8. Case 1: isosurface of dissolved CO_2 at 0.004 liquid mole fraction simulated by the FHM at 100 years, 500 years, and 1000 years with $\sigma^2 = 0.1$ (a–c) and $\sigma^2 = 4.5$ (d–f).

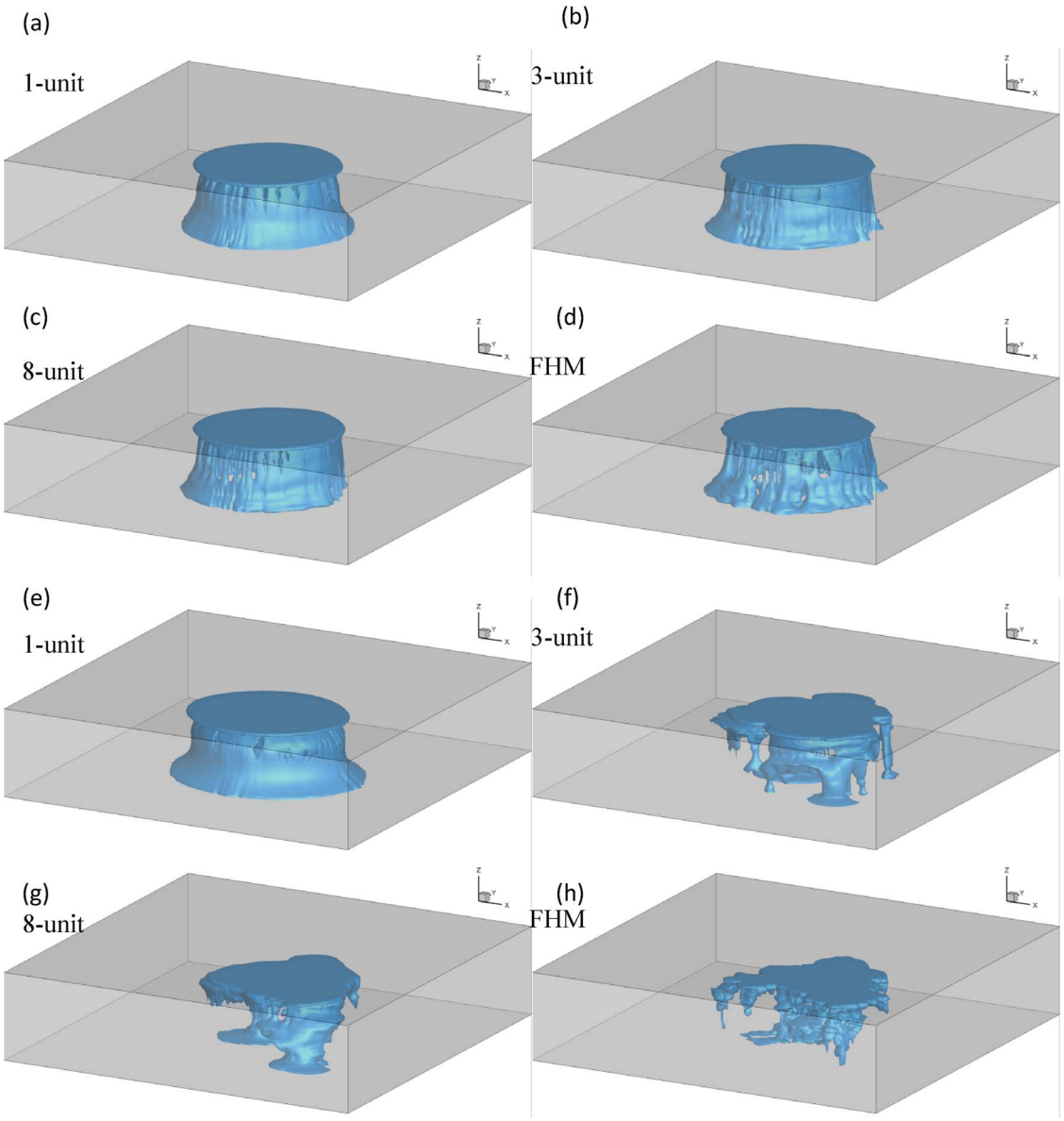

Fig. 9. Case 1: isosurface of dissolved CO_2 at 0.004 liquid mole fraction simulated by all models at 2000 years with $\sigma^2 = 0.1$ (a–d) and $\sigma^2 = 4.5$ (e and h).

variances. Most of the dissolved CO_2 accumulates beneath caprock in local equilibrium with $scCO_2$, the higher variance cases exhibiting more strongly irregular shapes. Strong aquifer heterogeneity ($\sigma^2 = 4.5$) clearly exerts an effect on the development of supercritical and dissolved CO_2 plumes. In contrast, when heterogeneity is weak ($\sigma^2 = 0.1$), FHM simulates a symmetric plume as predicted by analytic theories for homogeneous aquifers. Dissolved CO_2 simulated by all models are compared at the end of simulation, for the low- (Fig. 7a–d) and high-variance (Fig. 7e–h) cases. For the FHM, when variance is low, more fingering is observed at 2000 years (Fig. 7d) compared to its earlier plume shape (Fig. 6c); when variance is high, however, only minor difference is observed (Fig. 7h versus Fig. 6f). This suggests that fingering growth over time, thus dissolution storage, is promoted when aquifer is homogeneous or weakly heterogeneous, but is inhibited when the aquifer is strongly heterogeneous. When variance is high, *lateral* preferential flow paths arise from the interbedded horizontal to sub-horizontal high-k layers in the aquifer. Along these layers, $scCO_2$ and dissolved CO_2 migrate, resulting in an irregular dissolved plume dominated by advective transport. Within the intervening log-k layers, diffusion then dominates driven by the concentration gradient. The overall dynamics (advective transport dominates in high-k layers and diffusion dominates between high-k and low-k layers) act to suppress convective mixing.

For case 15, when variance is low, all HSMs can capture the dissolved plume shape and strength of fingering of the FHM, thus accurate predictions of the dissolved CO_2. When variance is high, however, HSMs of enhanced resolution (i.e., 3- and 8-unit models) are needed to capture the geometry of both the dissolved and $scCO_2$ (not shown) plumes. When comparing the 4 models (Fig. 7e–h), the higher the heterogeneity resolution, the more inhibited the dissolution fingering appears to be.

The above summary for case 25 may vary when a different parameter combination is evaluated. Results are examined for case 1 (Figs. 8 and 9), which, compared to case 25, has low salinity (more dissolution). Comparing Fig. 8 with Fig. 6, the FHM predicts more fingering and dissolution when aquifer variance is low, but no appreciable difference when aquifer variance is high. Clearly, high variance suppresses fingering even when the formation is saturated with freshwater. When comparing the 4 models (Fig. 9e–h), heterogeneity resolution is again found to significantly influence the development of fingering. Similar to what was observed for case 25, the higher the resolution, the more strongly inhibited dissolution fingering is. However, when variance is

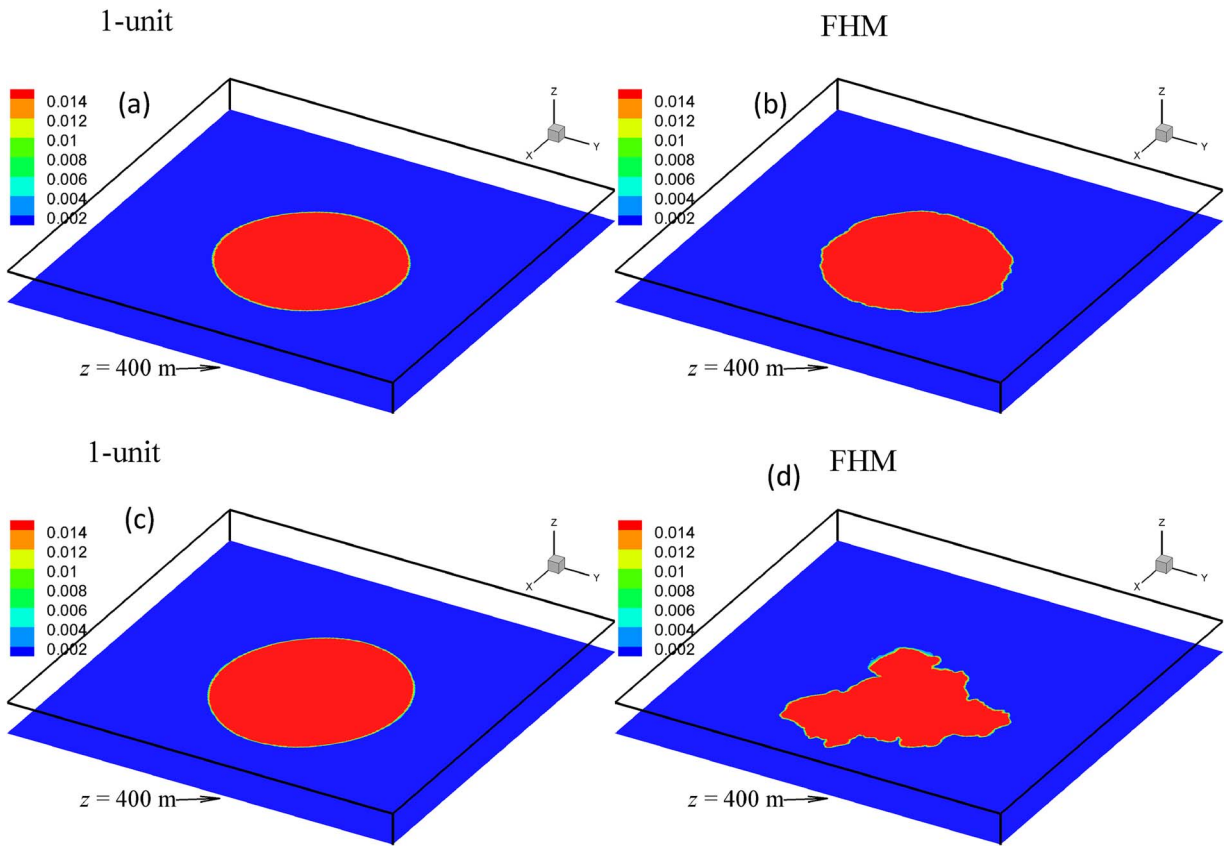

Fig. 10. Case 17: supercritical CO_2 saturation at 2000 years with $\sigma^2 = 0.1$ (a and b) and $\sigma^2 = 4.5$ (c and d) at the interface between aquifer and caprock. Predictions of the 1-unit model and the FHM are shown.

low (Fig. 9a–d), fingering is equally predicted by *all* models and heterogeneity resolution becomes less important. In summary, aquifer variance, heterogeneity resolution, and salinity all affect the development of fingering and dissolution storage.

3.3. Supercritical CO_2 footprint

A pool of $scCO_2$ forming a footprint beneath the caprock poses leakage risk, and the larger the footprint, the higher the risk. For case 17 (median salinity), CO_2 saturation predicted by the 1-unit model and the FHM at the end of simulation are plotted along the aquifer/caprock interface (Fig. 10). Results for both low and high variance cases are shown. When variance is low, the 1-unit model (also, the 3- and 8-unit models, not shown) can accurately depict the location, size, and shape of the $scCO_2$ footprint. Conversely, when variance is high, the 1-unit model fails to capture the strongly irregular $scCO_2$ footprint of the FHM. In this case, the 3-unit and 8-unit models (not shown) are better predictors.

3.4. Supercritical CO_2 pressure

Figs. 11–14 present $scCO_2$ pressure over time for case 25 (all parameters assume median values) at 4 observation points located at the center of the storage system at various depths (Fig. 1a). This is the region where formation pore pressure is expected to be the highest and where bottom-hole pressure can be monitored at the CO_2 injection well. At point A (z = 205 m; near the middle depth of the storage aquifer), for all variances, HSMs accurately predict the pressure profile of the FHM. At point B (z = 305 m; closer to caprock), all HSMs can again provide good prediction of the pressure change. Though there appears deviation between pressure profile of the FHM and those of the 1- and 3-unit models when σ^2 is 0.1, the relative error in pressure prediction is less than 1%. At point C, for all variances, the 8-unit model is the most accurate, followed by the 3-unit, and then the 1-unit model. Again, the relative error in pressure prediction is less than 1%. Similar observation is made for point D near the middle of the caprock. To summarize, pressure error of the HSMs appears to be affected by the position of the observation point, and it increases with variance and decreases with increasing heterogeneity resolution. Given that this error is generally very small, any HSM (with the 1-unit model being optimal) can provide reasonable pore pressure prediction.

3.5. Uncertainty analysis

For all models, two outputs at the end of simulation were analyzed with MANOVA: total dissolved CO_2 and total CO_2 leakage into caprock and overlying aquifer. In predicting each output, important parameters are ranked from the most important to the least important at 95% significance. Ranking statistics are then compiled for all models to evaluate parameter sensitivity for each output. For the ranges of the factors varied, salinity is the most important factor controlling CO_2 dissolution (Table 3), while caprock permeability and injection rate have minor impacts on dissolution. Temperature gradient is the least important. Decreasing salinity, increasing caprock permeability, and increasing injection rate lead to more dissolution. Caprock permeability is the most important factor controlling CO_2 leakage, followed by salinity, while effects of injection rate and temperature gradient are negligible (Table 4). While these results are more or less expected, a significant observation is that *the overall order of parameter ranking is relatively insensitive to either aquifer variance or heterogeneity resolution*. For a given variance, though the higher resolution HSMs can better capture the magnitudes of the ranking statistics of the FHM, sensitivity analysis conducted with any HSM can provide information on important parameters that impact the select performance metrics.

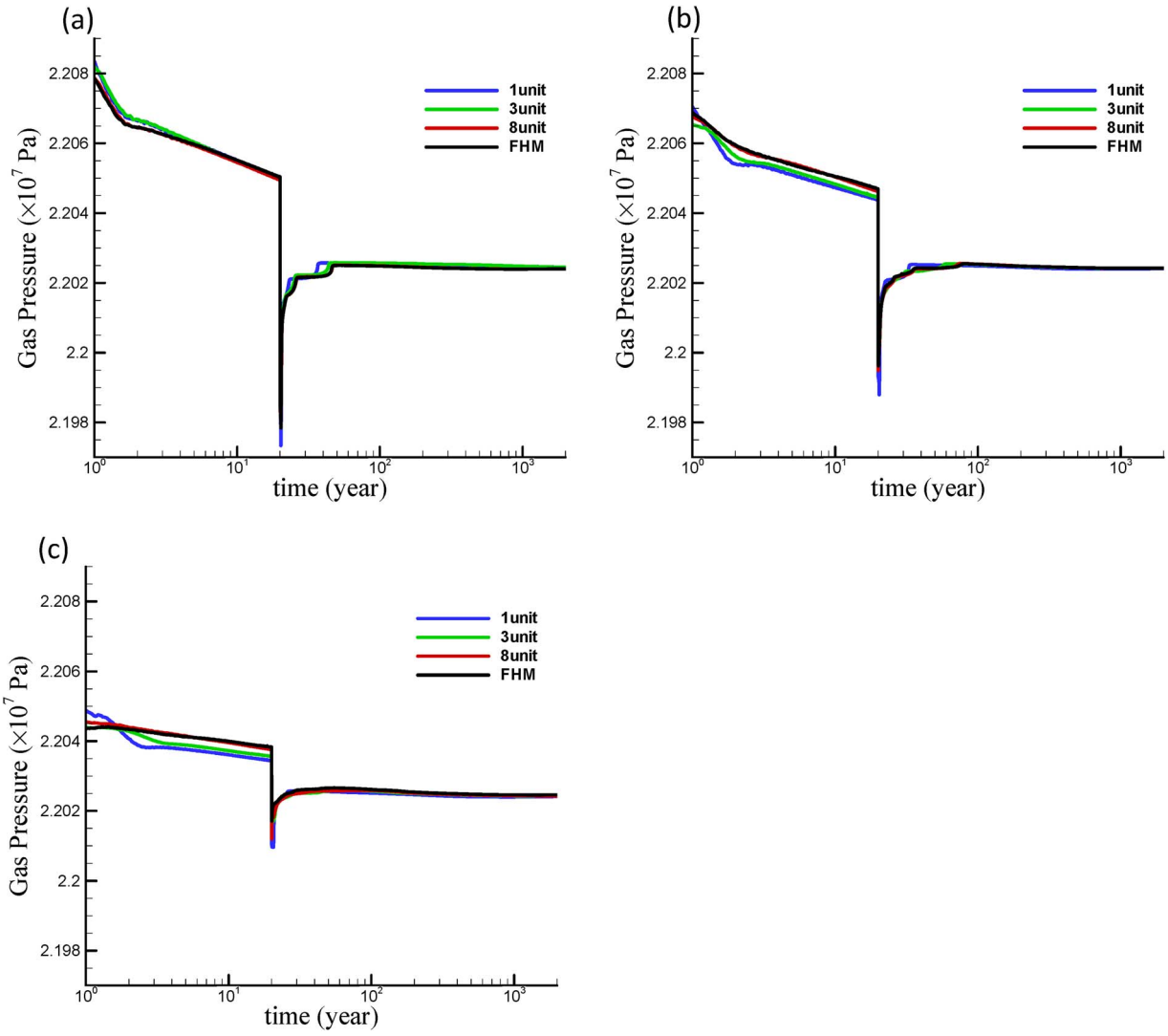

Fig. 11. Case 25: $scCO_2$ pressure profile at point A (z = 205m) with σ^2 = 0.1 (a), σ^2 = 1.0 (b), and σ^2 = 4.5 (c).

4. Discussion

Natural aquifers often exhibit permeability variation characterized with long-range connected (Bridge, 2003; Gershenzon et al., 2015b; Knudby and Carrera, 2005; Lunt et al., 2004; Wen and Gómez-Hernández, 1998; Zinn, 2003) or hierarchical heterogeneity (Bersezio et al., 1999; Jussel et al., 1994; Koltermann and Gorelick, 1996; Lu and Zhang, 2002; Tompson et al., 1998; Weissmann et al., 2002; Zhou et al., 2003). In building GCS models of deep aquifers, incorporating *k* heterogeneity down to the smallest resolvable continuum scale is impractical, due to lack of data, computational limitation, and economics (Friedmann and Stamp, 2006). Some level of small scale heterogeneity is always ignored, which leads to uncertainty about the conceptual site model, and in particular, how spatial variation of fluid flow parameters should be represented in model in order to evaluate CO_2 performance metrics. Though such models are frequently developed to estimate storage, project risk, and quantify uncertainty, conceptual model uncertainty is rarely considered. Can such models be used to accurately predict CO_2 storage, leakage, and reservoir pressure, as they occur in naturally heterogeneous aquifers? Moreover, uncertainty analysis, which is frequently used to evaluate model parameters, can be computationally demanding using large grids with multi-scale heterogeneity. Thus, can simplified conceptual models ignoring one or more scales of heterogeneity be useful for a parameter sensitivity analysis to identify key factors?

This study conducts CO_2 simulations and uncertainty analysis using synthetic models that capture heterogeneity at different resolutions. A FHM, derived from experimental data exhibiting high-resolution connected facies, provides a reference. Based on this model, equivalent permeability tensors were computed for 3 HSMs with a global upscaling technique that accounts for irregular facies shapes. Because HSMs can be built using different data involving different levels of site characterization, our goal is to evaluate conceptual model uncertainty. By conducting a parameter uncertainty analysis using all models, we aim to (1) evaluate whether HSMs can make reasonably accurate calculations of CO_2 performance metrics under different parametric combinations; and (2) whether the HSMs can be used in a sensitivity analysis to identify and rank uncertainty factors. Among the performance metrics, outcomes related to both $scCO_2$ and dissolved CO_2 are of interest, thus two-phase simulation was dynamically coupled to the simulation of single-phase convective mixing, i.e., variable density flow of brine variably saturated with CO_2.

Despite the outcomes suggesting the usefulness of the HSMs, the new insights must be interpreted within a proper theoretical framework with several limitations in mind. The HSMs were created to capture permeability connectivity in three dimensions using an image algorithm. They were created based on *complete* knowledge of permeability heterogeneity which is required to compute the equivalent permeabilities. In practice, HSMs are frequently built using logging or seismic

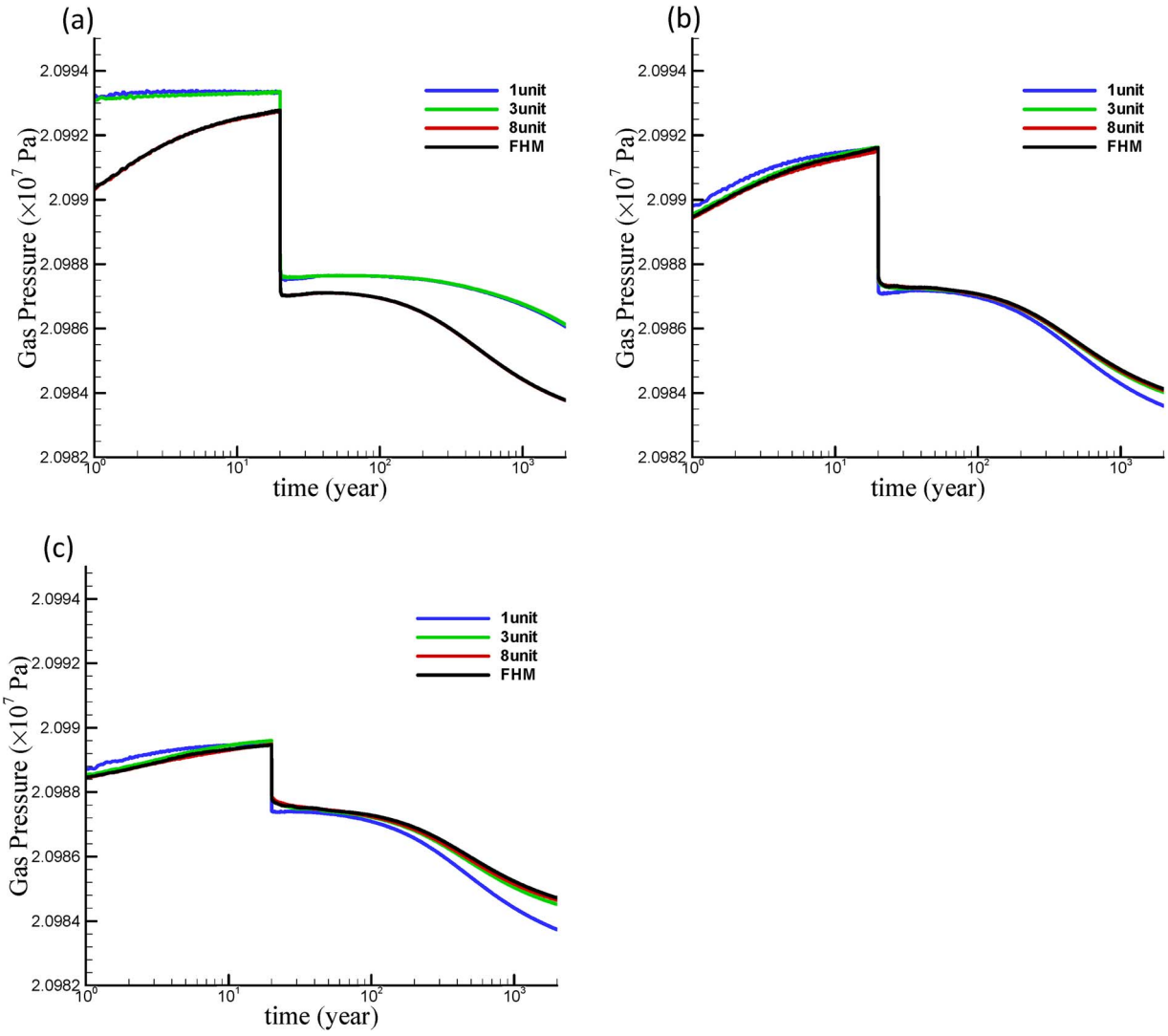

Fig. 12. Case 25: $scCO_2$ pressure profile at point B (z = 305m) with σ^2 = 0.1 (a), σ^2 = 1.0 (b), and σ^2 = 4.5 (c).

data that are sensitive to formation lithology but not necessarily sensitive to permeability groupings. Such models can also exhibit significant uncertainty in capturing facies connectivity in regions away from wells. The estimation of equivalent permeabilities of irregular facies based on *limited data* requires additional research. Moreover, an identical, high-resolution grid was used by all models to eliminate errors that can arise from different discretizations (such errors can be significant when ln*k* variance is high). However, real-world HSMs are usually discretized with coarse grids so simulations can be completed within a reasonable time. HSMs of this study thus represent best-case scenarios where a target aquifer has been extensively characterized. As this scenario is rarely possible when building models for deep aquifers, performance of real-world HSMs will likely degrade depending on their accuracy in incorporating facies geometry, permeability, and use of appropriately refined grids. However, our study approach – from the permeability upscaling method to the DoE sensitivity analysis – is easily extendible to problems with different heterogeneity, operating condition, and leakage scenarios, e.g., one or more faults or leaky wells can be placed in overburden. Thus, a useful outcome of this study is to illustrate a systematic approach for evaluating conceptual model uncertainty when multiple models can be developed for a storage site.

Finally, for some scenarios evaluated in this study (e.g., low aquifer variability and/or high salinity), the HSMs can calculate similar fluid pressure and CO_2 footprint as the FHM, suggesting that history matching using fluid pressure and plume sizes alone will likely lead to non-unique identification of formation permeability. Given different parameterization choices, in order to capture the effect of underlying variability, the estimation procedure *should* also lead to scale-dependent permeabilities with variable anisotropies. How such permeabilities could be scaled for hierarchical aquifers was discussed in Zhang et al. (2011) in detail and is not elaborated herein.

5. Conclusions

This study models CO_2 injection and post-injection monitoring at high resolution in three-dimensions to evaluate long-term dissolution, leakage, footprint, and pore pressure evolution in a storage system including a target aquifer, caprock, and an overlying aquifer. Using PFLOTRAN, a highly scalable, parallel multiphase multicomponent simulator running on a NCAR-Wyoming supercomputer, miscible two-phase flow is explicitly simulated to account for CO_2 injection and single-phase convective mixing. Because permeability heterogeneity can influence both single- and two-phase flows, and because heterogeneity is often represented in site models at various resolutions depending on the availability of characterization data, CO_2 simulations

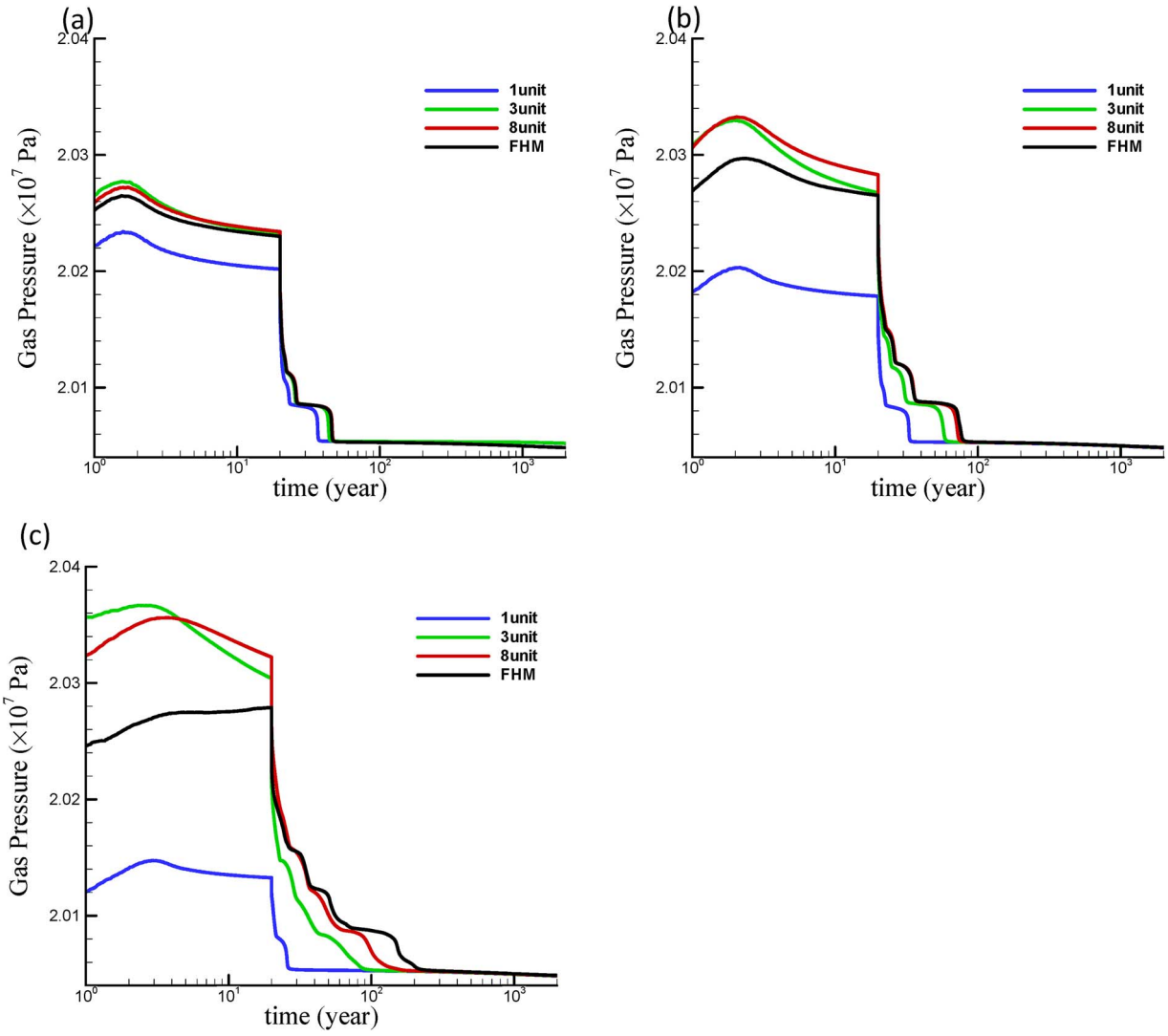

Fig. 13. Case 25: $scCO_2$ pressure profile at point C (z = 395m) with σ^2 = 0.1 (a), σ^2 = 1.0 (b), and σ^2 = 4.5 (c).

were conducted using a suite of synthetic aquifer models including a reference FHM incorporating high resolution permeability heterogeneity and 3 HSMs with reduced heterogeneity resolution and upscaled permeabilities. To understand the uncertainty in predicting long-term dissolution and leakage, a computationally efficient sensitivity analysis was carried out using all models. Among 4 parameters varied (geothermal gradient, salinity, caprock permeability, and injection rate), those with a first order impact on long-term dissolution and leakage were identified. The determination of "optimal" heterogeneity resolution, which can lead to model simplification, was thus evaluated within a designed parameter space. Because natural aquifers can exhibit variable degrees of heterogeneity, the analysis was repeated at increasing ln*k* variances. For the modeling choices, assumptions, and the chosen ranges of the input parameters varied, our study insights are summarized in the following:

1. Aquifer variance, heterogeneity resolution, and salinity can all affect the development of dissolution fingering, convective mixing, and thus the amount of long term dissolution.
2. The 3-unit HSM appears adequate for capturing both supercritical and dissolved plume dynamics of the FHM, the amount of CO_2 leakage, and reservoir pore pressure. This model is the all-around optimal model.
3. The 1-unit model is adequate for calculating formation pore pressure in response to injection and post-injection migration. When aquifer variability is low, it is also adequate for capturing the extent of supercritical and dissolved CO_2 footprints and CO_2 leakage. However, this model is inaccurate when: (a) salinity is low (convective mixing is overestimated), and (b) aquifer variability is high (preferential flow is not captured). Interestingly, the 1-unit model preserves the parameter ranking of the FHM for all ln*k* variances, suggesting that it is an *optimal* model for a parameter sensitivity analysis.
4. The order of parameter ranking is relatively insensitive to aquifer variance and heterogeneity resolution (i.e., uncertainty in conceptual model), thus HSMs of *any* resolution may be effectively utilized for a sensitivity analysis.
5. The amount of CO_2 dissolution is mostly controlled by brine salinity, while leakage is mostly controlled by caprock permeability. This observation is largely independent of the conceptual model tested and the underlying aquifer variability.

This study suggests that "optimal" models with reduced heterogeneity resolution likely exist for site screening purposes, which can lead to significant savings for sites with limited data. Compared to the reference model with 3.2 million individual permeabilities, the HSMs are assigned 1–8 equivalent permeabilities to represent the underlying heterogeneities. However, HSM of real world aquifers will suffer from uncertainty in its capture of connected facies away from well control.

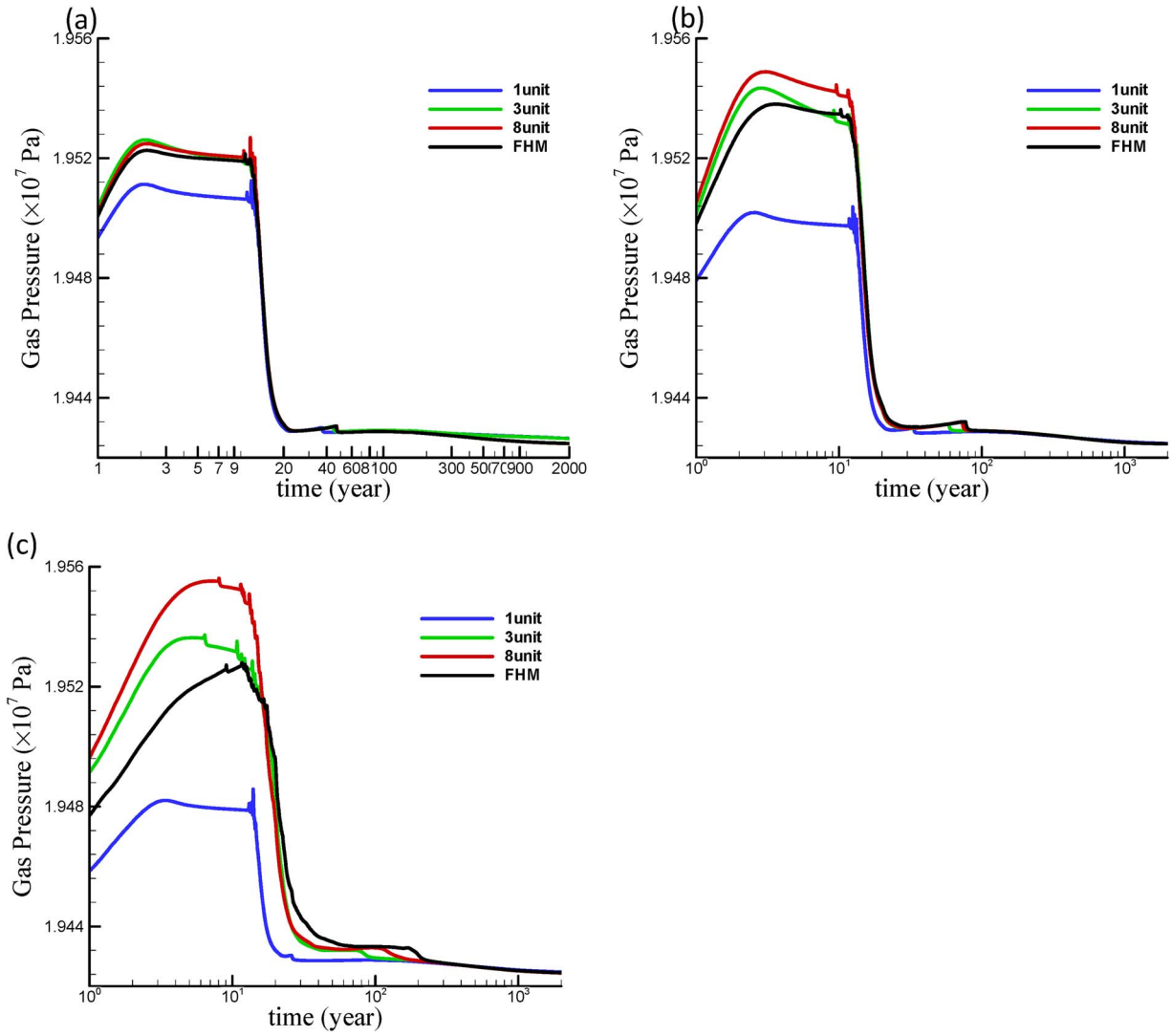

Fig. 14. Case 25: $scCO_2$ pressure profile at point D (z = 455 m) with σ^2 = 0.1 (a), σ^2 = 1.0 (b), and σ^2 = 4.5 (c).

Table 3
Parameter ranking for predicting the total dissolved CO_2 at the end of the simulation. Plot estimates graphically present the relative impact of a factor: bar extending to the left indicates that increasing value of a factor leads to decreasing dissolution, and vice versa.

	σ^2 = 0.1		σ^2 = 1.0		σ^2 = 4.5	
Model	Term	Plot Estimate	Term	Plot Estimate	Term	Plot Estimate
1unit	T Gradient		T Gradient		T Gradient	
	Brine Salinity		Brine Salinity		Brine Salinity	
	K Cap		K Cap		K Cap	
	Inj rate		Inj rate		Inj rate	
3unit	T Gradient		T Gradient		T Gradient	
	Brine Salinity		Brine Salinity		Brine Salinity	
	K Cap		K Cap		K Cap	
	Inj rate		Inj rate		Inj rate	
8unit	T Gradient		T Gradient		T Gradient	
	Brine Salinity		Brine Salinity		Brine Salinity	
	K Cap		K Cap		K Cap	
	Inj rate		Inj rate		Inj rate	
FHM	T Gradient		T Gradient		T Gradient	
	Brine Salinity		Brine Salinity		Brine Salinity	
	K Cap		K Cap		K Cap	
	Inj rate		Inj rate		Inj rate	

Table 4
Parameter ranking for predicting the total leaked CO_2 at the end of the simulation. Plot estimates graphically present the relative impact of a factor.

	$\sigma^2 = 0.1$		$\sigma^2 = 1.0$		$\sigma^2 = 4.5$	
Model	Term	Plot Estimate	Term	Plot Estimate	Term	Plot Estimate
1unit	T Gradient		T Gradient		T Gradient	
	Brine Salinity		Brine Salinity		Brine Salinity	
	K Cap		K Cap		K Cap	
	Inj rate		Inj rate		Inj rate	
3unit	T Gradient		T Gradient		T Gradient	
	Brine Salinity		Brine Salinity		Brine Salinity	
	K Cap		K Cap		K Cap	
	Inj rate		Inj rate		Inj rate	
8unit	T Gradient		T Gradient		T Gradient	
	Brine Salinity		Brine Salinity		Brine Salinity	
	K Cap		K Cap		K Cap	
	Inj rate		Inj rate		Inj rate	
FHM	T Gradient		T Gradient		T Gradient	
	Brine Salinity		Brine Salinity		Brine Salinity	
	K Cap		K Cap		K Cap	
	Inj rate		Inj rate		Inj rate	

Real-world HSM is typically discretized with coarse grids. Thus, their performance will likely degrade in comparison with the high-resolution HSMs developed based on complete knowledge of aquifer permeability. Future research will focus on developing inverse methods to identify dominant facies or pathways in a storage system and to estimate their equivalent permeabilities. Thus, permeability upscaling, employed in this work to demonstrate the existence of 'optimal' models, would be unnecessary. A novel aquifer inverse method for data-poor systems is under development, where facies and permeability can be simultaneously identified for deep aquifers with unknown fluid flow boundary conditions (Jiao and Zhang, 2016). The synthetic models developed herein can be used to test and verify inverse methods.

Acknowledgements

The research carried out in this work was supported by the U.S. Department of Energy, Office of Fossil Energy, Grant number DE-FE-0009238. We would also like to acknowledge the use of computational resources (ark:/85065/d7wd3xhc) at the NCAR-Wyoming Supercomputing Center, which are provided by the National Science Foundation and the State of Wyoming and are supported by NCAR's Computational and Information Systems Laboratory. We thank two anonymous reviewers for their helpful comments in improving the manuscript.

References

Agartan, E., Trevisan, L., 2015. Experimental study on effects of geologic heterogeneity in enhancing dissolution trapping of supercritical CO2. Water Resour. Res. 51, 1635–1648. http://dx.doi.org/10.1002/2014WR015778.

Balay, S., Gropp, W.D., McInnes, L.C., Smith, B.F., 1997. Efficient management of parallelism in object oriented numerical software libraries. In: Arge, E., Bruaset, A.M., Langtangen, H.P. (Eds.), Modern Software Tools in Scientific Computing. Birkhäuser Press, pp. 163–202.

Barrash, W., Clemo, T., 2002. Hierarchical geostatistics and multifacies systems: Boise hydrogeophysical research site, Boise, Idaho. Water Resour. Res. 38 (10).

Battiato, I., Tartakovsky, D.M., Tartakovsky, A.M., Scheibe, T.D., 2011. Hybrid models of reactive transport in porous and fractured media. Adv. Water Resour. 34, 1140–1150. http://dx.doi.org/10.1016/j.advwatres.2011.01.012.

Bersezio, R., Bini, A., Giudici, M., 1999. Effects of sedimentary heterogeneity on groundwater flow in a quaternary pro-glacial delta environment: joining facies analysis and numerical modelling. Sediment. Geol. 129 (3), 327–344. http://dx.doi.org/10.1016/s0037-0738(98)00145-6.

Bouzgarrou, S., Harzallah, H.S., Slimi, K., 2013. Unsteady double diffusive natural convection in porous media-application to CO2 storage in deep saline aquifer reservoirs. Energy Procedia 36, 756–765. http://dx.doi.org/10.1016/j.egypro.2013.07.088.

Bridge, J.S., 2003. Rivers and Floodplains: Form, Process, and Sedimentary Record. Wiley-Blackwell.

CISL, 2013. 2013 CISL Annual Report.

Chen, C., Zeng, L., Shi, L., 2013. Continuum-scale convective mixing in geological CO2 sequestration in anisotropic and heterogeneous saline aquifers. Adv. Water Resour. 53, 175–187. http://dx.doi.org/10.1016/j.advwatres.2012.10.012.

Chevalier, S., Faisal, T.F., Bernabe, Y., Juanes, R., Sassi, M., 2015. Numerical sensitivity analysis of density driven CO2 convection with respect to different modeling and boundary conditions. Heat Mass Transf. 51, 941–952. http://dx.doi.org/10.1007/s00231-014-1466-2.

Class, H., Helmig, R., Neuweiler, I., 2008. Sequential coupling of models for contaminant spreading in the vadose zone. Vadose Zo. J. 7, 721. http://dx.doi.org/10.2136/vzj2007.0056.

Court, B., Bandilla, K.W., Celia, M. a., Janzen, A., Dobossy, M., Nordbotten, J.M., 2012. Applicability of vertical-equilibrium and sharp-interface assumptions in CO 2 sequestration modeling. Int. J. Greenh. Gas Control 10, 134–147. http://dx.doi.org/10.1016/j.ijggc.2012.04.015.

Datta-Gupta, A., King, M., 2007. Streamline Simulation: Theory and Practice. Society Of Petroleum Engineers.

Duan, Z., Sun, R., 2003. An improved model calculating CO 2 solubility in pure water and aqueous NaCl solutions from 273 to 533 K and from 0 to 2000 bar. Chem. Geol. 193, 257–271.

Duan, Z., Hu, J., Li, D., Mao, S., 2008. Densities of the CO2–H2O and CO2–H2O–NaCl systems up to 647 K and 100 MPa. Energy Fuels 22, 1666–1674.

Elenius, M.T., Gasda, S.E., 2013. Convective mixing in formations with horizontal barriers. Adv. Water Resour. 62, 499–510. http://dx.doi.org/10.1016/j.advwatres.2013.10.010.

Ennis-King, J.P., Paterson, L., 2005. Role of convective mixing in the long-term storage of carbon dioxide in deep saline formations. SPE J. 10, 349–356. http://dx.doi.org/10.2118/84344-PA.

Ertekin, T., Abou-Kassem, J.H., King, G.R., 2001. Basic Applied Reservoir Simulation, SPE Textbook Series Vol. 7. 406 pp.

Farajzadeh, R., Salimi, H., Zitha, P.L.J., Bruining, H., 2007. Numerical simulation of density-driven natural convection in porous media with application for CO2 injection projects. Int. J. Heat Mass Transf. 50, 5054–5064. http://dx.doi.org/10.1016/j.ijheatmasstransfer.2007.08.019.

Flett, M., Gurton, R., Weir, G., 2007. Heterogeneous saline formations for carbon dioxide disposal: impact of varying heterogeneity on containment and trapping. J. Pet. Sci. Eng. 57, 106–118. http://dx.doi.org/10.1016/j.petrol.2006.08.016.

Friedmann, S.J., Stamp, V.W., 2006. Teapot dome: characterization of a CO2-enhanced oil recovery and storage site in Eastern Wyoming. Environ. Geosci. 13, 181–199. http://dx.doi.org/10.1306/eg.01200605017.

Fritz, J., Flemisch, B., Helmig, R., 2012. Decoupled and multiphysics models for non-isothermal compositional two-phase flow in porous media. Int. J. Numer. Anal. Model. 9, 17–28.

Gasda, S.E., Nordbotten, J.M., Celia, M.A., 2009. Vertical equilibrium with sub-scale analytical methods for geological CO2 sequestration. Comput. Geosci. 13, 469–481. http://dx.doi.org/10.1007/s10596-009-9138-x.

Gasda, S.E., Nordbotten, J.M., Celia, M.A., 2011. Vertically averaged approaches for CO 2 migration with solubility trapping. Water Resour. Res. 47, W05528. http://dx.doi.org/10.1029/2010WR009075.

Gasda, S.E., Nordbotten, J.M., Celia, M. a., 2012. Application of simplified models to CO 2 migration and immobilization in large-scale geological systems. Int. J. Greenh. Gas Control 9, 72–84. http://dx.doi.org/10.1016/j.ijggc.2012.03.001.

Gasda, S.E., Nilsen, H.M., Dahle, H.K., 2013. Impact of structural heterogeneity on up-scaled models for large-scale CO2 migration and trapping in saline aquifers. Adv. Water Resour. 62, 520–532. http://dx.doi.org/10.1016/j.advwatres.2013.05.003.

Gaus, I., 2010. Role and impact of CO2-rock interactions during CO2 storage in sedimentary rocks. Int. J. Greenh. Gas Control 4, 73–89. http://dx.doi.org/10.1016/j.ijggc.2009.09.015.

Geiger, S., Lord, G., Tambue, A., 2012. Exponential time integrators for stochastic partial differential equations in 3D reservoir simulation. Comput. Geosci. 16, 323–334. http://dx.doi.org/10.1007/s10596-011-9273-z.

Gershenzon, N., Ritzi, R., Dominic, D., 2015a. Influence of small-scale fluvial architecture on CO2 trapping processes in deep brine reservoirs. Water Resour. 51 (10),

8240–8256. http://dx.doi.org/10.1002/2015WR017638.
Gershenzon, N., Soltanian, M., Ritzi, R., 2015b. Understanding the impact of open-framework conglomerates on water-oil displacements: the Victor interval of the Ivishak Reservoir, Prudhoe Bay Field, Alaska. Petroleum Geosci. 21 (1) 43. http://dx.doi.org/10.1144/petgeo2014-017.
Hassanzadeh, H., Pooladi-Darvish, M., Keith, D.W., 2007. Scaling behavior of convective mixing, with application to geological storage of CO2. AIChE J. 53, 1121–1131. http://dx.doi.org/10.1002/aic.11157.
Hidalgo, J.J., MacMinn, C.W., Juanes, R., 2013. Dynamics of convective dissolution from a migrating current of carbon dioxide. Adv. Water Resour. 62, 511–519. http://dx.doi.org/10.1016/j.advwatres.2013.06.013.
IPCC, 2005. IPCC special report on carbon dioxide capture and storage. IPCC Special Report on Carbon Dioxide Capture and Storage.
Islam, A.W., Sharif, M.A.R., Carlson, E.S., 2013. Numerical investigation of double diffusive natural convection of CO2 in a brine saturated geothermal reservoir. Geothermics 48, 101–111. http://dx.doi.org/10.1016/j.geothermics.2013.07.001.
Jiao, J., Zhang, Y., 2016. Direct method of hydraulic conductivity structure identification for subsurface transport modeling. J. Hydrol. Eng. 21 (10) 04016033:1–14.
Juanes, R., Lie, K.-A., 2006. Numerical modeling of multiphase first-contact miscible flows. Part 1. Analytical Riemann solver. Transp. Porous Media 67, 375–393. http://dx.doi.org/10.1007/s11242-006-9031-1.
Juanes, R., Lie, K.-A., 2007. Numerical modeling of multiphase first-contact miscible flows. Part 2. Front-tracking/streamline simulation. Transp. Porous Media 72, 97–120. http://dx.doi.org/10.1007/s11242-007-9139-y.
Jun, Y.-S., Giammar, D.E., Werth, C.J., 2013. Impacts of geochemical reactions on geologic carbon sequestration. Environ. Sci. Technol. 47, 3–8. http://dx.doi.org/10.1021/es3027133.
Jussel, P., Stauffer, F., Dracos, T., 1994. Transport modeling in heterogeneous aquifers: 1. Statistical description and numerical generation of gravel deposits. Water Resour. Res. 30, 1803–1817. http://dx.doi.org/10.1029/94WR00162.
Knudby, C., Carrera, J., 2005. On the relationship between indicators of geostatistical, flow and transport connectivity. Adv. Water Resour. 28, 405–421. http://dx.doi.org/10.1016/j.advwatres.2004.09.001.
Koltermann, C.E., Gorelick, S.M., 1996. Heterogeneity in sedimentary deposits: a review of structure-imitating, process-imitating, and descriptive approaches. Water Resour. Res. 32, 2617–2658. http://dx.doi.org/10.1029/96WR00025.
Lazaro Vallejo, L., Leahy, M.J., Dance, T., LaForce, T.C., 2011. New phase behavior algorithm for simulation of CO_2 storage. In: SPE Reservoir Simulation Symposium. Society of Petroleum Engineers. http://dx.doi.org/10.2118/141734-MS.
Li, S., Zhang, Y., 2014. Model complexity in carbon sequestration: a design of experiment and response surface uncertainty analysis. Int. J. Greenh. Gas Control 22, 123–138. http://dx.doi.org/10.1016/j.ijggc.2013.12.007.
Li, S., Zhang, Y., Zhang, X., Du, C., 2012. Geologic modeling and fluid-flow simulation of acid gas disposal in western Wyoming. Am. Assoc. Pet. Geol. Bull. 96, 635–664. http://dx.doi.org/10.1306/07261110178.
Li, S., Akbarabadi, M., Zhang, Y., Piri, M., 2016. An integrated site characterization-to-optimization study for commercial-scale carbon dioxide storage. Int. J. Greenh. Gas Control 44, 74–87. http://dx.doi.org/10.1016/j.ijggc.2015.10.003.
Lichtner, P.C., Hammond, G.E., Lu, C., Karra, S., Bisht, G., Andre, B., Mills, R.T., Kumar, J., 2013. PFLOTRAN. Web page [WWW Document]. URL http://www.pflotran.org/.
Lu, Z., Zhang, D., 2002. On stochastic modeling of flow in multimodal heterogeneous formations. Water Resour. Res. 38http://dx.doi.org/10.1029/2001WR001026. 8-1–8-15.
Lu, C., Han, W.S., Lee, S.Y., McPherson, B.J., Lichtner, P.C., 2009. Effects of density and mutual solubility of a CO2-brine system on CO2 storage in geological formations: warm vs. cold formations. Adv. Water Resour. 32, 1685–1702. http://dx.doi.org/10.1016/j.advwatres.2009.07.008.
Lunt, I., Bridge, J., Tye, R., 2004. A quantitative, three-dimensional depositional model of gravelly braided rivers. Sedimentology 51 (3), 377–414. http://dx.doi.org/10.1111/j.1365-3091.2004.00627.x.
MacMinn, C.W., Neufeld, J. a., Hesse, M. a., Huppert, H.E., 2012. Spreading and convective dissolution of carbon dioxide in vertically confined, horizontal aquifers. Water Resour. Res. 48, 1–11. http://dx.doi.org/10.1029/2012WR012286.
Martinez, M.J., Hesse, M.A., 2016. Two-phase convective CO 2 dissolution in saline aquifers. Water Resour. Res. 52, 585–599. http://dx.doi.org/10.1002/2015WR017085.
Milliken, W., Levy, M., Strebelle, S., 2008. The effect of geologic parameters and uncertainties on subsurface flow: deepwater depositional systems. SPE West. Reg. 1–16.
Montgomery, D., 2008. Design and Analysis of Experiments, seventh ed. John Wiley & Sons.
Neuweiler, I., Papafotiou, A., Class, H., Helmig, R., 2011. Estimation of effective parameters for a two-phase flow problem in non-Gaussian heterogeneous porous media. J. Contam. Hydrol. 120–121, 141–156. http://dx.doi.org/10.1016/j.jconhyd.2010.08.001.
Nield, D. a., Kuznetsov, a. V., Simmons, C.T., 2010. The effect of strong heterogeneity on the onset of convection in a porous medium: 2d/3d localization and spatially correlated random permeability fields. Transp. Porous Media 83, 465–477. http://dx.doi.org/10.1007/s11242-009-9455-5.
Niessner, J., Helmig, R., 2009. Multi-physics modeling of flow and transport in porous media using a downscaling approach. Adv. Water Resour. 32, 845–850. http://dx.doi.org/10.1016/j.advwatres.2009.02.007.
Parker, J., 2010. Algorithms for Image Processing and Computer Vision.
Pau, G.S.H., Bell, J.B., Pruess, K., Almgren, A.S., Lijewski, M.J., Zhang, K., 2010. High-resolution simulation and characterization of density-driven flow in CO2 storage in saline aquifers. Adv. Water Resour. 33, 443–455. http://dx.doi.org/10.1016/j.advwatres.2010.01.009.
Qi, R., LaForce, T.C., Blunt, M.J., 2009a. Design of carbon dioxide storage in aquifers. Int. J. Greenh. Gas Control 3, 195–205. http://dx.doi.org/10.1016/j.ijggc.2008.08.004.
Qi, R., LaForce, T.C., Blunt, M.J., 2009b. A three-phase four-component streamline-based simulator to study carbon dioxide storage. Comput. Geosci. 13, 493–509. http://dx.doi.org/10.1007/s10596-009-9139-9.
Ranganathan, P., Farajzadeh, R., Bruining, H., Zitha, P.L.J., 2012. Numerical simulation of natural convection in heterogeneous porous media for CO2 geological storage. Transp. Porous Media 95, 25–54. http://dx.doi.org/10.1007/s11242-012-0031-z.
Rhodes, M.E., Bijeljic, B., Blunt, M.J., 2008. Pore-to-field simulation of single-phase transport using continuous time random walks. Adv. Water Resour. 31, 1527–1539. http://dx.doi.org/10.1016/j.advwatres.2008.04.006.
Riaz, A., Hesse, M., Tchelepi, H.A., Orr, F.M., 2005. Onset of convection in a gravitationally unstable diffusive boundary layer in porous media. J. Fluid Mech. 548, 87–111. http://dx.doi.org/10.1017/S0022112005007494.
Ryan, E.M., Tartakovsky, A.M., 2011. A hybrid micro-scale model for transport in connected macro-pores in porous media. J. Contam. Hydrol. 126, 61–71. http://dx.doi.org/10.1016/j.jconhyd.2011.06.005.
Sheets, B.A., Hickson, T.A., Paola, C., 2002. Assembling the stratigraphic record: depositional patterns and time-scales in an experimental alluvial basin. Basin Res. 14, 287–301. http://dx.doi.org/10.1046/j.1365-2117.2002.00185.x.
Soltanian, M., Ritzi, R., 2014. A new method for analysis of variance of the hydraulic and reactive attributes of aquifers as linked to hierarchical and multiscaled sedimentary architecture. Water Resour. Res. 50 (12), 9766–9776. http://dx.doi.org/10.1002/2014WR015468.
Soltanian, M.R., Amooie, M.A., Dai, Z., Cole, D., Moortgat, J., 2016. Critical dynamics of gravito-convective mixing in geological carbon sequestration. Sci. Rep. 6, 35921. http://dx.doi.org/10.1038/srep35921.
Span, R., Wagner, W., 1996. A new equation of state for carbon dioxide covering the fluid region from the triple-point temperature to 1100 K at pressures up to 800 MPa. J. Phys. Chem. Ref. Data 25, 1509–1596.
Tartakovsky, A.M., Tartakovsky, D.M., Meakin, P., 2008. Stochastic Langevin model for flow and transport in porous media. Phys. Rev. Lett. 101, 44502. http://dx.doi.org/10.1103/PhysRevLett.101.044502.
Tartakovsky, A.M., 2010. Langevin model for reactive transport in porous media. Phys. Rev. E 82, 26302. http://dx.doi.org/10.1103/PhysRevE.82.026302.
Tilton, N., Riaz, A., 2014. Nonlinear stability of gravitationally unstable, transient, diffusive boundary layers in porous media. J. Fluid Mech. 745, 251–278. http://dx.doi.org/10.1017/jfm.2014.72.
Tilton, N., Daniel, D., Riaz, A., 2013. The initial transient period of gravitationally unstable diffusive boundary layers developing in porous media. Phys. Fluids 25, 92107. http://dx.doi.org/10.1063/1.4821225.
Tompson, A.F.B., Falgout, R.D., Smith, S.G., Bosl, W.J., Ashby, S.F., 1998. Analysis of subsurface contaminant migration and remediation using high performance computing. Adv. Water Resour. 22, 203–221. http://dx.doi.org/10.1016/S0309-1708(98)00013-X.
Tyagi, M., Jenny, P., 2011. Probability density function modeling of multi-phase flow in porous media with density-driven gravity currents. Transp. Porous Media 87, 603–623. http://dx.doi.org/10.1007/s11242-010-9704-7.
Tyagi, M., Jenny, P., Lunati, I., Tchelepi, H.A., 2008. A Lagrangian, stochastic modeling framework for multi-phase flow in porous media. J. Comput. Phys. 227, 6696–6714. http://dx.doi.org/10.1016/j.jcp.2008.03.030.
Weissmann, G.S., Zhang, Y., LaBolle, E.M., Fogg, G.E., 2002. Dispersion of groundwater age in an alluvial aquifer system. Water Resour. Res. 38, 16-1-16-13. http://dx.doi.org/10.1029/2001WR000907.
Wen, X.H., Gómez-Hernández, J.J., 1998. Numerical modeling of macrodispersion in heterogeneous media: a comparison of multi-Gaussian and non-multi-Gaussian models. J. Contam. Hydrol. 30, 129–156. http://dx.doi.org/10.1016/S0169-7722(97)00035-1.
Yeten, B., Castellini, A., Guyaguler, B., Chen, W.H., 2005. A comparison study on experimental design and response surface methodologies. In: SPE Reservoir Simulation Symposium. Society of Petroleum Engineers. http://dx.doi.org/10.2118/93347-ms.
Zhang, Y., Gable, C.W., Person, M., 2006. Equivalent hydraulic conductivity of an experimental stratigraphy: implications for basin-scale flow simulations. Water Resour. Res. 42, 1–19. http://dx.doi.org/10.1029/2005wr004720. W05404.
Zhang, Y., Gable, C.W., Sheets, B., 2010. Equivalent hydraulic conductivity of three-dimensional heterogeneous porous media: an upscaling study based on an experimental stratigraphy. J. Hydrol. 388, 304–320. http://dx.doi.org/10.1016/j.jhydrol.2010.05.009.
Zhang, Y., Liu, B., Gable, C.W., 2011. Homogenization of hydraulic conductivity for hierarchical sedimentary deposits at multiple scales. Transp. Porous Media 87, 717–737. http://dx.doi.org/10.1007/s11242-010-9711-8.
Zhang, Y., Yang, G., Li, S., 2014. Significance of Conceptual model uncertainty in simulating carbon sequestration in a deep inclined saline aquifer. Hazard. Toxic Radioact. Waste.
Zhang, W., 2013. Effect of modeling factors on the dissolution-diffusion-convection process during CO2 geological storage in deep saline formations. Front. Earth Sci. 7, 238–256. http://dx.doi.org/10.1007/s11707-013-0359-x.
Zhou, Q., Liu, H.H., Bodvarsson, G.S., Oldenburg, C.M., 2003. Flow and transport in unsaturated fractured rock: effects of multiscale heterogeneity of hydrogeologic properties. J. Contam. Hydrol. 60, 1–30. http://dx.doi.org/10.1016/S0169-7722(02)00080-3.
Zinn, B., 2003. When good statistical models of aquifer heterogeneity go bad: a comparison of flow, dispersion, and mass transfer in connected and multivariate Gaussian hydraulic conductivity fields. Water Resour. Res. 39http://dx.doi.org/10.1029/2001WR001146. SBH 4-0-4-4.